Cooperative Spectrum Sensing and Fusion Based on Tangle Networks

Shuang Zheng, Yuna Jiang, Xiaohu Ge, *Senior Member, IEEE,* Yong Xiao, *Senior Member, IEEE,* Yang Huang, Yuan Liu

***Abstract*—Cooperative spectrum sensing (CSS) is a promising solution to improve the spectrum sensing performance. However, some cooperative secondary users (SUs) may intentionally send wrong spectrum sensing results for the benefit of themselves, which will bring security problems to the CSS-enabled systems. Besides, the behavior of the primary user (PU) may change dynamically when SUs sense the spectrum, which affects the accuracy of CSS. In this paper, a CSS architecture based on the Tangle blockchain is proposed, where massive mobile devices (MDs) act as spectrum sensing nodes and blockchain nodes. A novel dynamic spectrum sensing algorithm is proposed based on the mean-field game. A two-step spectrum sensing fusion mechanism based on the age of information (AoI) and cumulative weight (CW) of transactions is proposed to address the impact of perceptual data differences on the overall decision. The simulation results show that, compared with the traditional fixed spectrum sensing strategy, the MDs' weighted sensing utility in the proposed dynamic spectrum sensing scheme is improved by 10% on average. Moreover, compared to the traditional maximal ratio combining fusion mechanism, the detection probability of the proposed two-step spectrum sensing fusion mechanism is maximally increased by 30.23%, and the false alarm probability is minimally reduced by 9.92%.**

***Index Terms*—Cooperative Spectrum Sensing, Mean Field Game, Tangle, Sensing Fusion, Age of Information.**

I. INTRODUCTION

With the explosive growth in the number of mobile devices (MDs), the traditional static spectrum allocation and management mechanisms have been considered as one of the major obstacles to support resource-demanding services and applications for next-generation wireless communication networks [1], [2]. Cooperative Spectrum Sensing (CSS) is regarded as an effective solution to alleviate the spectrum shortage and underutilization [3]. By allowing secondary users (SUs) to sense the status of primary users (PUs) before accessing the licensed spectrum [4], the throughput and utilization of spectrum resources of the SUs can be improved without causing adverse effects to the PUs [5]. A fusion center can be deployed to fuse spectrum sensing results of multiple SUs to further improve sensing accuracy. Recent results suggest that by adopting proper fusing rules at the fusion center, the spectrum sensing accuracy can be significantly improved, even in a low signal-to-noise ratio (SNR) scenario [6]–[9]. However, most existing works only consider the optimization of spectrum sharing strategies and often ignore the security issues in sensing result fusion, e.g., some malicious SUs intentionally send wrong spectrum sensing results for the benefit of themselves [10]. Besides, the centralized database maintained by the fusion center may be vulnerable to the single point of failure. It is necessary to design a security-enhanced solution for CSS that does not have to rely on a centralized result fusion.

Blockchain is considered to be a promising solution due to its advantages of transparency, autonomy and traceability [11]. Based on the blockchain technology, all the spectrum sharing interactions among entities in large-scale wireless networks can be managed in a tamper-proof and decentralized way. The consensus mechanism is a critical part of the blockchain, and refers to the process of achieving agreement on the state of data among the network participants [12]. Proof-of-work (PoW) and proof-of-stake (PoS) are the two of the most common consensus mechanisms. Unfortunately, these two consensus mechanisms suffer from low transaction throughput and high transaction fees, making them unsuitable for spectrum sharing in large-scale wireless networks [12]. The direct acyclic graph (DAG) consensus mechanism is an emerging solution that has the potential to relax the single-chain constraint. So the newly issued transactions can be quickly added to the ledger, thus improving transaction throughput and consensus delay of blockchain deployed in a large networking system [13]. Tangle is a DAG consensus-based blockchain solution. In Tangle, each transaction has an initial self-weight and cumulative weight (CW). The self-weight of a transaction is proportional to the amount of work that the issuing node invested into it. The cumulative weight (CW) is defined as the self-weight of a particular transaction plus the sum of self-weights of all transactions that directly or indirectly approve this transaction [14]. CW of transactions can reflect the acceptance of transactions by Tangle networks. The markov chain monte carlo (MCMC) algorithm [15] is

This work was supported by the National Natural Science Foundation of China under Grant U2001210, the National Natural Science Foundation of China under Grant No. 62071193, the Key R & D Program of Hubei Province of China under Grant No. 2021EHB015 and 2020BAA002.

Shuang Zheng, Yuna Jiang and Xiaohu Ge (Corresponding author) are with School of Electronic Information and Communications, Huazhong University of Science and Technology, Wuhan, 430074, Hubei, China and Shenzhen Huazhong University of Science and Technology Research Institute, Shenzhen, 518063, Guangdong, China. Xiaohu Ge is also with China International Joint Research Center of Green Communications and Networking. (e-mail: s_zheng@hust.edu.cn, yunajiang@hust.edu.cn, xhge@mail.hust.edu.cn).

Yong Xiao is with the School of Electronic Information and Communications at the Huazhong University of Science and Technology, Wuhan, China. Yong Xiao is also with the Pengcheng National Lab (Guangzhou Base), Guangzhou, China and China International Joint Research Center of Green Communications and Networking, Wuhan, China. (e-mail: yongxiao@hust.edu.cn).

Yang Huang is with the School of Information and Communication Engineering, Nanjing University of Aeronautics and Astronautics, Nanjing, 211100, Jiangsu, China (e-mail: yang.huang.ceie@nuaa.edu.cn).

Yuan Liu is with the School of Electronic and Information Engineering, South China University of Technology, Guangzhou, 510641, Guangdong, China (e-mail: eeyliu@scut.edu.cn).

often adopted in Tangle networks to add new transactions to the ledger. Compared to PoW and PoS mechanisms, Tangle is a promising solution to the blockchain scalability issues. Besides, Tangle offers much faster transaction verification speed and improved transaction throughput, and is therefore a more suitable solution when being applied into decentralized CSS in large-scale wireless networks. None of existing studies investigate the decentralized CSS based on Tangle networks.

When the sensing nodes in large-scale wireless networks continuously increase, the application of classical game theory to solve the optimal strategy of each sensing node will greatly increase the complexity of the optimal strategy. Therefore, the spectrum sensing mechanisms proposed in the existing CSS studies are not suitable for the CSS in wireless networks with a large number of sensing nodes. As a mathematical tool, the mean field game is applicable for wireless networks with a large number of game players [16]–[18]. The mean field game is a promising solution to address the individual's interaction with the effect of collective behavior of players, and may reduce the complexity of solving the optimized strategies in large-scale wireless networks. It has already been applied to optimize power control [19] and user scheduling [20], [21] problems in wireless communication networks. However, the mean field game is rarely applied in the research field of CSS. Considering that the MDs need to consume energy in the CSS and the energy of massive MDs is limited, the optimal spectrum sensing strategy of massive MDs should be dynamically adjusted according to the change of residual energy. It is still challenging to employ the mean field game to solve the optimal sensing strategy of massive MDS with energy constraints.

Besides, an effective fusion mechanism in the CSS is required to fuse the spectrum sensing results of all MDs when the spectrum sensing process is performed by a large number of MDs. In the current spectrum sensing process, the status of PUs in the spectrum sensing can dynamically change, and the sensing result can only reflect the current state of PUs' occupancy in the licensed spectrum. Age of information (AoI) is a popular metric to measure the freshness of the received information. It is defined as the time that elapsed since the last update has been received. AoI of MDs' sensing results is critical for the final fusion results in the CSS, as the fresh sensing results are more consistent with the actual spectrum occupancy situation. Outdated sensing results may lead to the lower accuracy of the final sensing fusion results. There are few studies considering the AoI in the fusion mechanism of CSS.

To mitigate above challenges, in this paper, we develop a novel CSS architecture based on the Tangle blockchain. In this architecture, the dynamic spectrum sensing decision making process is formulated as a mean field game. Besides, we propose a new two-step spectrum sensing fusion mechanism based on the AoI and CW of transactions in Tangle. The main contributions of this paper are summarized as follows:

- A CSS architecture for the large-scale wireless networks is proposed based on the Tangle blockchain, and each MD performs both spectrum sensing and transactions consensus. All the spectrum sensing interactions and results are recorded on blockchain distributed ledger, which can resist MDs' malicious tampering behaviors.
- Given the limited energy and sensing utility function of massive MDs, an optimal dynamic spectrum sensing strategy for massive MDs based on the mean field game is proposed.
- Considering that the state of PU changes dynamically and perceptual data in different time slots have different impacts on the overall decision, a new two-step spectrum sensing fusion mechanism based on the AoI and CW of transactions is proposed.
- The simulation results demonstrate that, compared with the traditional maximal ratio combining fusion mechanism, the detection probability of the proposed two-step spectrum sensing fusion mechanism can be improved by 30.23%, and the false alarm probability can be reduced by 9.92%.

The remaining of the paper is organized as follows. Related works are described in Section II. The system model is given in Section III. In Section IV, sensing utility expressions of massive MDs are derived. In Section V, the process of solving the optimization problem of sensing utility based on the mean field game is introduced. In Section VI, the spectrum sensing fusion mechanism based on the AoI and CW is designed. In section VII, numerical results of the proposed spectrum sensing and fusion mechanism are analyzed. Finally, the paper is concluded in the last Section.

II. Related Works

A. Cooperative Spectrum Sensing Schemes

There are some studies investigating the cooperative spectrum sensing. Some works focus on the deep learning-based CSS. The authors in [22] proposed deep reinforcement learning-based CSS algorithm to decrease the signaling overhead in the networks of SUs. To improve the sensing accuracy of SUs, the authors in [23] proposed a cooperative sensing algorithm, a multi-agent deep deterministic policy gradient algorithm was employed to reduce the synchronization and communication overhead. In [24], the authors proposed a federated learning-based spectrum sensing algorithm. Each SU employs local data to train the neural network model and sends the gradient to the fusion center to integrate the system parameters. In [25], the authors combine CSS with deep learning to detect potential illegal drones with states of high uncertainty. In [26], the authors employed the distributed deep reinforcement learning method to learn the optimal CSS strategy. The coordination graph is used to decompose the problem into a max-plus problem. Considering that SUs may consume energy when sensing spectrum, CSS needs to design an effective incentive mechanism to encourage SU to join in the CSS, so as to maximize the spectrum sensing utilization [27]. The authors in [28] proposed an incentive mechanism based on contract theory, in which the interaction between SUs and PUs has been formulated as a labor market. The authors in [29] proposed a distributed dynamic load balancing clustering algorithm to reduce the network energy consumption and improve the detection probability of spectrum sensing. The game theory

[30] has also been widely used in the design of spectrum sensing mechanism in the CSS. An incentive mechanism based on Stackelberg game is proposed in [31]. In the Leader game, the fusion center motivates the sensing user to join the CSS by providing the optimal reward. In the Follower game, after receiving the reward issued by the fusion center, the SUs can adjust its spectrum sensing strategy to get more profits. The authors in [32] proposed a CSS incentive mechanism based on non-cooperative game, and the authors in [33] adopted the non-cooperative Nash-bargaining game for the spectrum sensing benefit analysis of SUs and PUs in the CSS.

There are few existing studies focusing on the application of blockchain to CSS [34]–[36], most of which introduce the blockchain architecture based on PoW or PoS consensus. The authors in [34] propose Sensechain, which uses the distributed consensus mechanism in the blockchain network to capture the reputation of SU, and identify the malicious SU based on reputation evaluation. Similarly, the authors in [35] also use blockchain to select spectrum sensing nodes. Besides, in order to incentivize SU to participate in the spectrum senisng and PoW process, the spectrum access opportunity is provided as a reward for SUs, and the optimal strategy solution of this sensing-access-consensus architecture is proposed in [36]. However, the applicability of traditional blockchain architecture in terms of throughput and latency in large-scale CSS scenarios has not been widely considered in existing studies.

B. Fusion Mechanisms in Cooperative Spectrum Sensing

An effective fusion mechanism in the CSS is required to fuse the spectrum sensing results of all MDs. The authors in [37] derived the closed expression of detection probability under different channel models, and simulated the performance under different hard decision fusion rules. The authors in [38] proposed a new hard decision fusion, which treated the optimization result of cluster head's non-cooperative game sensing strategy as a necessary condition in the fusion mechanisms. Simulation results show that this scheme can improve the global detection probability and reduce the error detection probability. A soft decision fusion scheme based on entropy weight was proposed in [39], which divided SUs into different clusters, and adopted equal weight fusion within clusters to improve the detection probability. The detection probability and false alarm probability of traditional Maximal Ratio Combining (MRC), Selective Combining (SC) and other soft fusion mechanisms are compared in [40].

III. System Model

As shown in Fig. 1, the set of MDs is denoted as $\mathcal{M} = \{1, \ldots, m, \ldots M\}$, and the locations of MDs follows Poisson distribution. The MDs are considered as spectrum sensing nodes in the CSS. Without loss of generality, the Base Station (BS) in the cellular network operated in the licensed spectrum is regarded as PU. In this paper, a PU in the cellular network is randomly selected to analyze the spectrum sensing utilization in the large-scale CSS scenarios. Massive MDs not only act as the spectrum sensing nodes in the CSS to jointly sense the state of PU, but also act as the blockchain node in Tangle networks to propose and validate transactions. There are mainly three kinds of transactions in Tangle networks: tips, unconfirmed and fully confirmed. Tips are newly attached transactions that have not been referenced by other transactions. Unconfirmed transactions are those waiting to be confirmed. Fully confirmed transactions are considered as confirmed if they have already been directly or indirectly referenced by all tips. When a new transaction wants to join tangle networks, it needs to reference and approve two existing transactions. This rule defines the underlying structure of Tangle networks. All nodes in Tangle networks can participate in the consensus, which increases network security. Before the spectrum sensing process, the PU will publish the smart contract to Tangle networks, which define some basic rules about spectrum allocation. During the spectrum sensing process, MDs adopt different sampling frequency strategies to sense the spectrum. As the reward for MDs to participate in the CSS, the specific frequency band is allocated to MDs according to the contribution of MDs in the way of Time division multiple access (TDMA). After MDs make the spectrum sensing strategies, MDs send transactions containing the spectrum sensing strategy to Tangle networks. The transaction information will be synchronized at every node in the Tangle network. Then each MD can compute its own time allocation result based on the smart contract published by PU and other MDs' sensing strategies.

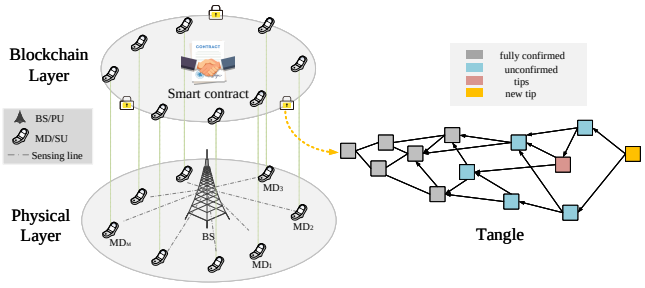

Fig. 1: System model.

Without loss of generality, a frame structure for periodic sensing by MDs was designed in this paper as shown in Fig 2. Each frame T_f includes three parts: the sensing stage T_s, the consensus stage T_c and the transmission stage T_{tr}. The length of frame T_f satisfies T_f=T_s+T_c+T_{tr}. The MDs would consume the energy during the sensing stage and the energy of massive MDs is limited. Meanwhile, the dynamic change of the PU's state will influence the accuracy of the spectrum sensing results. In this paper, the sensing stage T_s is divided into the small instantaneous sensing time slots δ. It is assumed that each MD will dynamically adjust its sensing sampling strategy according to its remaining energy in the instantaneous sensing time slot δ. When δ is infinitesimal, it can be approximately regarded as a continuous sensing process. Therefore, the sensing sampling strategy of the MD $m(m \in \mathcal{M})$ at the time of $t\,(0 \leq t \leq T_s)$ is denoted as $f_m\,(t)$.

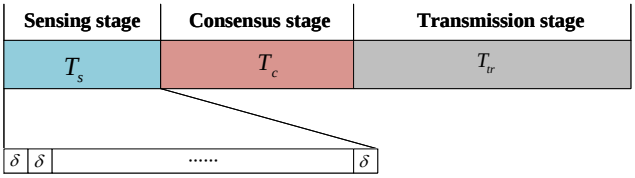

Fig. 2: The frame structure of the spectrum sensing.

The main architecture of this article is shown in Fig. 3. We mainly focus on the CSS and spectrum fusion stage. In the CSS stage, all MDs will sense spectrum based on mean field game and send their sensing results as a transaction to the smart contract in the Tangle, then step into the consensus stage. In the spectrum fusion stage, a new two-step spectrum sensing fusion mechanism based on the AoI and CW of transactions is proposed. The first step is that MD performs local fusion, in which sensing results of each time slot in the sensing stage is fused based on AoI. Besides, all the transactions sent by MDs have accumulated different CW during the consensus stage, thus the second step of the fusion mechanism is to integrate the sensing results of all MDs based on the CW. After the consensus, all MDs step into the data transmission stage. This paper focuses on the sensing and consensus stage, and the data transmission stage is not within the scope of this paper.

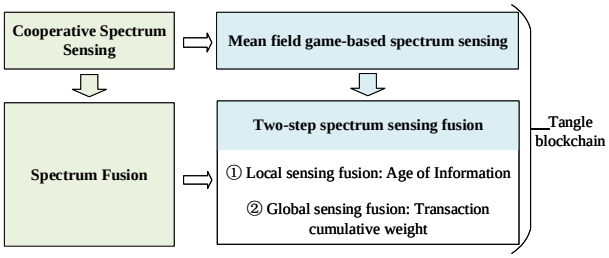

Fig. 3: Tangle blockchain-enabled CSS and spectrum fusion.

IV. Formulation of Sensing Utility Function

A. Sensing Utility Function

The access time of a specific frequency band (such as unlicensed frequency band) is treated as a reward for MDs, and the specific frequency band is allocated in the way of TDMA according to the contribution of MDs. During the spectrum sensing process, MDs adopt different sampling frequency strategies. Higher sampling frequency may result in higher detection probability, which also leads to more energy consumption of MDs. So, the detection probability can reflect the contribution of MDs in the CSS. Here, the detection probability is the probability that MDs' detection results are correct, and is expressed as [6]

$$Pd_m\left(f_m\left(t\right)\right)=Q\left(\frac{Q^{-1}\left(Pf_m\right)-\gamma_m\left(t\right)\sqrt{f_m\left(t\right)\delta}}{\sqrt{2\gamma_m\left(t\right)+1}}\right), \quad (1)$$

where Pf_m is the false alarm probability that the sensing decision of m is occupation while PU does not occupy the authorized frequency band. δ is the small instantaneous sensing slot. The SNR when m is sensing is denoted as $\gamma_m\left(t\right)$. $Q\left(x\right)=\frac{1}{\sqrt{2\pi}}\int_x^{\infty}e^{-\frac{t^2}{2}}dt$ is Gaussian Q-Function. The contribution ratio of MD m to the spectrum sensing can be expressed as $Pd_m\left(f_m\left(t\right)\right)/\sum_{j=1}^{M}Pd_j\left(f_j\left(t\right)\right)$. So, the usable time of m in the specific frequency band can be provided by $T_u\times Pd_m\left(f_m\left(t\right)\right)/\sum_{j=1}^{M}Pd_j\left(f_j\left(t\right)\right)$, in which the total available time of this specific frequency band is denoted as T_u. MDs that get higher detection probability can obtain longer access time, which ensures fairness among MDs. The sensing revenue $b_m\left(t\right)$ of m at time t is defined as the revenue that can be obtained from data transmission in this specific frequency band and is expressed as

$$b_m\left(t\right)=T_u\times\frac{Pd_m\left(f_m\left(t\right)\right)}{\sum_{j=1}^{M}Pd_j\left(f_j\left(t\right)\right)}\times R_m w_m, \quad (2)$$

where w_m is the revenue per bit of transmission. The transmission rate at which m occupies the specific frequency band is expressed as

$$R_m=\log\left(1+\frac{p_m^u h_m^u (r_m^u)^{-a}}{\sigma_n^2}\right), \quad (3)$$

where p_m^u is the transmission power of m over the specific frequency band, and the bandwidth of this specific frequency band is normalized to 1. r_m^u is the distance between m and the receiver. The average power of the interference noise is σ_n^2, the path loss coefficient is α. We assume that the fast fading is Rayleigh fading, and h_m^u follows an exponential distribution with parameter 1, which is expressed as $h_m^u\sim\exp\left(1\right),\forall m\in M$. The sensing cost $c_m\left(t\right)$ of m is defined as the energy consumed by spectrum sensing in the sensing time slot δ

$$c_m\left(t\right)=a_2 p_m^s f_m\left(t\right)\delta, \quad (4)$$

where p_m^s is the energy consumption of a single sampling in spectrum sensing, a_2 is the cost per unit of energy. The sensing utility of m at time t is expressed as

$$\begin{aligned}U_m\left(f_m\left(t\right)\right)&=a_1 b_m\left(t\right)-a_2 c_m\left(t\right)\\&=a_1 T_u\frac{Pd_m(f_m(t))}{\sum_{j=1}^{M}Pd_j(f_j(t))}R_m w_m-a_2 p_m^s f_m\left(t\right)\delta\ ,\end{aligned} \quad (5)$$

where a_1 is the utility coefficient.

B. Mean Field Game Formulation

The optimal sensing strategy for MD is to maximize the sensing utility function. At any time t, the control strategy set A_m is given by

$$A_m=\left\{f_m\left(t\right)|f_m\left(t\right)\in\left[f_{min},f_{max}\right]\right\}, \quad (6)$$

where $f_m(t)$ is the sensing sampling strategy of m in time t, f_{min} is minimum sampling frequency and f_{max} is the maximum sampling frequency that MD can take. Since the remaining energy of m is gradually reduced due to the continuous sensing and sampling in the sensing process, the state

$e_m(t)\,(0 \le e_m(t) \le E_{max})$ of m is defined as the dynamic change of the remaining energy with the time in the sensing process.

$$e_m(t) = E_{max} - p_m^s f_m(t)\delta, \tag{7}$$

where E_{max} is the maximum sensing energy of MDs during one spectrum sensing progress. The change of state is expressed by

$$de_m(t) = -p_m^s f_m(t)dt. \tag{8}$$

According to Equation (8), the state of MD is controlled by a differential equation related to energy, and the optimization objective function F of m is expressed as

$$\begin{aligned} F = &\max_{f_m(0\to T_s)} E\left[\int_0^{T_s} U_m\left(f_m\left(t,e_m\right)\right)dt\right] \\ s.t.&\begin{cases} de_m(t) = -p_m^s f_m(t,e_m)\,dt, 0 \le t \le T_s \\ f_m(t,e_m) \in [f_{\min}, f_{\max}] \end{cases} \end{aligned} \tag{9}$$

where $f_m(0 \to T_s)$ represents the curve of sampling frequency used by m in the time period T_s from the initial time. $f_m(t,e_m)$ is the sensing sampling frequency used by m in the time t and the remaining energy e_m. $U_m(f_m(t,e_m))$ is the utility of m when the sensing sampling is $f_m(t,e_m)$.

The solution of the objective function F is the optimal strategies set of all MDs $\mathcal{F}^* = [f_1^*(0\to T_s),\cdots,f_m^*(0\to T_s),\cdots,f_M^*(0\to T_s)]$, and $f_m^*(0\to T_s)$ is the optimal control strategy of m, which satisfies

$$\begin{aligned} &f_m^*(0\to T_s) = \arg\max_{f_m^*(0\to T_s)} E[\int_0^{T_s} U_m(f_m(t,e_m),\mathbf{f}_{-m}^*(t))dt] \\ &s.t.\begin{cases} de_m(t) = -p_m^s f_m(t,e_m)\,dt, 0 \le t \le T_s \\ f_m(t,e_m) \in [f_{\min}, f_{\max}] \\ e_m > 0 \end{cases} \end{aligned} \tag{10}$$

where $\mathbf{f}_{-m}^*(t)$ is the optimal sensing strategies set of all MDs except m.

The above optimization problem can be modeled as a stochastic differential game [41], and the Nash equilibrium solution of the stochastic differential game is the optimal sensing sampling frequency of MDs. In this paper, the value function $V_m(t,e_m(t))$ is defined as the maximum value of the objective function F from time t to T_s when m adopts different control strategies. $V_m(t,e_m(t))$ is expressed as

$$V_m(t,e_m(t)) = \max_{f_m(t\to T_s)} E[\int_t^{T_s} U_m\left(f_m\left(\tau,e_m\left(t\right)\right)\right)d\tau]. \tag{11}$$

According to the reference [19], the value function satisfies a Hamilton-Jacobi-Bellman (HJB) equation. In this paper, the HJB equation satisfying the equation of state as shown in Equation (8) is expressed as follows

$$\begin{aligned} &\frac{\partial V_m(t,e_m(t))}{\partial t} \\ &+ \max_{f_m(t,e_m)}\left[U_m\left(f_m\left(t,e_m\right)\right) - p_m^s f_m(t,e_m)\frac{\partial V_m(t,e_m(t))}{\partial e}\right] = 0 \end{aligned} \tag{12}$$

Theorem 1: The Nash equilibrium solution of the stochastic differential game exists.

Proof: See Appendix A.

V. Optimization of Network Sensing Utility

A. Sensing Utility Derivation Based on Mean Field Game

In order to find the Nash equilibrium point above, the partial differential equations with the same number of MDs has been derived in this paper. When the number of MDs is large, it is very difficult to solve the differential equations with a large number. Thus, we use the mean field game [16] to solve the problem of optimal sensing strategy for MDs in the CSS. The mean field (MF) $m(t,e)$ is expressed as

$$m(t,e) = \lim_{M\to\infty}\frac{1}{M}\sum_{\forall m} I_{\{e_m(t)=e\}}, \tag{13}$$

where $I_{\{e_m(t)=e\}}$ means that the value of the function is 1 when the state of m at time t is e. MF is the probability distribution of the state of MDs. The accuracy of the above approximation increases by increasing the number of MDs, as the effect of decision making to a single MD on the whole population becomes negligible. $U_{mean}(t,e)$ is the utility function under MF in the time t and remaining energy e. Considering that the receiver of MD moves within a certain range, the average of $U_{mean}(t,e)$ are obtained over the communication range of MDs and is expressed as

$$\begin{aligned} &U_{mean}(t,e) \\ &= E\left[U_m(t,e)\right] \\ &= a_1 T_u w_m \frac{Pd_m(f_m(t,e_m))E\left[\log\left(1+\frac{p_m^u h_m^u (r_m^u)^{-\alpha}}{\sigma_n^2}\right)\right]}{Pd_m(f_m(t,e_m)) + \sum_{j=1,j\ne m}^{M} Pd_j(f_j(t,e_j))} \\ &\quad - a_2 p_m^s f_m(t,e_m)\,\delta \end{aligned}, \tag{14}$$

where $U_m(t,e)$ is the utility of m in the time t and the remaining energy e, and

$$\begin{aligned} &E\left[\log\left(1+\frac{p_m^u h_m^u r_m^u(t)^{-\alpha}}{\sigma_n^2}\right)\right] \\ &= \int_{w>0}\Pr\left(\log\left(1+\frac{p_m^u h_m^u (r_m^u)^{-\alpha}}{\sigma_n^2}\right) > w\right)dw \\ &= \int_{w>0}\Pr\left(\frac{p_m^u h_m^u (r_m^u)^{-\alpha}}{\sigma_n^2} > e^w - 1\right)dw \\ &= \int_{r_m^u>0} e^{-\frac{(e^w-1)\sigma_n^2 (r_m^u)^{-\alpha}}{p_m^u}} 2\pi\lambda_u r_m^u e^{-\pi\lambda_u (r_m^u)^2} dr_m^u \end{aligned} \tag{15}$$

According to Rayleigh fading characteristics, h_m^u follows an exponential distribution with parameter 1. The distance r_m^u from the receiver of m satisfies the probability density distribution $f(r_m^u) = 2\pi\lambda_u r_m^u e^{-\pi\lambda_u (r_m^u)^2}$, in which the location of the user on the receiver follows a Poisson distribution of density λ_u. In this paper, $\sum_{j=1,j\ne m}^{M} Pd_j(f_j(t,e_j))$ in Equation (14) is defined as interference term $I_m(t)$. Under MF, interference term $I_m(t)$ is derived as

$$\begin{aligned} I_m^{mean}(t) &= E\left[\sum_{j=1,j\ne m}^{M} Pd_j(f_j(t,e_j))\right] \\ &\overset{M\to\infty}{\approx} (M-1)\,E^{mean}\left[Pd_j(f_j(t,e_j))\right] \end{aligned} \tag{16}$$

in which the mean value of detection probability under MF when the sensing strategy of the MD j is $f_j(t,e_j)$ is expressed as $E^{mean}\left[Pd_j(f_j(t,e_j))\right]$. Since the detection probability is

a function of γ_j, the detection probability $Pd_j\left(f_j\left(t,e_j\right)\right)$ is expressed as [42]

$$Pd_j\left(f_j\left(t,e_j\right)\right)=\int_0^{+\infty} Pd_j\left(f_j\left(t,e_j\right),\gamma_j\left(t\right)\right)f\left(\gamma_j\left(t\right)\right)d\gamma, \tag{17}$$

in which $f\left(\gamma_j\left(t\right)\right)=\frac{1}{\bar{\gamma}}\exp\left(-\frac{\gamma_j(t)}{\bar{\gamma}}\right)$ and $\bar{\gamma}$ is the average SNR. The detection probability under mean field is derived as

$$\begin{aligned}&E^{mean}\left[Pd_j\left(f_j\left(t,e_j\right)\right)\right]=\\&\int_0^{+\infty}\left(\int_e Q\left(\frac{Q^{-1}(Pf_j)-\gamma_j(t)\sqrt{f_j(t,e_j)\delta}}{\sqrt{2\gamma_j(t)+1}}\right)m\left(t,e\right)de\right)f\left(\gamma\right)d\gamma.\end{aligned} \tag{18}$$

Thus, the sensing utility of m under the mean field is given in (19). Based on the establishment of mean field, m can obtain its optimal sensing sampling strategy according to its own state $e_m(t)$ and mean field distribution $m(t,e)$. Thus, the sensing utility optimization problem of MD is transformed into

$$\begin{aligned}&\max_{f_m(0\to T_s)}\ E[\int_0^{T_s}U_m^{mean}\left(f_m\left(t,e_m\right),m\left(t,e\right)\right)dt]\\&s.t.\begin{cases}de_m\left(t\right)=-p_m^s f_m\left(t,e_m\right)dt, 0\le t\le T_s\\ f_m\left(t,e_m\right)\in[f_{\min},f_{\max}]\\ e_m>0\end{cases}\end{aligned} \tag{20}$$

B. Optimal Solution of Network Sensing Strategy Based on Mean Field Game

According to the character of mean field game, the numerical solution of Nash equilibrium of mean field game can be obtained by solving two equations composed of HJB and Fokker-Planck-Kolmogorov(FPK). The HJB equation is expressed as

$$\begin{aligned}&\tfrac{\partial V_m(t,e_m)}{\partial t}+\max_{f_m(0\to T_s)}(U_m^{mean}(f_m\left(t,e_m\right),m\left(t,e_m\right))\\&-p_m^s\cdot f_m\left(t,e_m\right)\cdot\tfrac{\partial V_m(t,e_m)}{\partial e})=0.\end{aligned} \tag{21}$$

The FPK equation is expressed as

$$\frac{\partial m(t,e_m)}{\partial t}-p_m^s\cdot\frac{\partial}{\partial e}(m(t,e_m)f_m(t,e_m))=0. \tag{22}$$

The above two equations can remove the subscript m to obtain the following simplified equations.

$$\begin{aligned}&\tfrac{\partial V(t,e)}{\partial t}+\\&\max_{f(0\to T_s)}(U^{mean}(f\left(t,e\right),m\left(t,e\right))-p^s f\left(t,e\right)\tfrac{\partial V(t,e)}{\partial e})=0\end{aligned} \tag{23}$$

$$\frac{\partial m(t,e)}{\partial t}-p^s\cdot\frac{\partial}{\partial e}(m(t,e)f(t,e))=0. \tag{24}$$

By solving the above two equations, the optimal sensing strategy control curve $f\left(0\to T_s\right)$ and the state change curve $m(t,e)$ of MD at any time can be obtained.

In order to solve the optimal sensing strategy solution of the above mean field game, the time axis and state space into a space with $(X+1)\cdot(Y+1)$ points are discretized [19]. The interval between every two time points δ and the interval between two state points δ_e are respectively given by

$$\delta=\frac{T_s}{X}\ ,\quad \delta_e=\frac{E_{\max}}{Y}. \tag{25}$$

Algorithm 1 Iterative algorithm for calculating Nash equilibrium point in mean field game

Input: The initial value of the value function $V\left(X,j\right)=0.05\exp\left(Y-\delta_e j\right)$ and the initial value of mean field $m\left(i,j\right)=\frac{1}{X+1}, i=1,2,\ldots,X+1; j=1,2,\ldots,Y+1$;

Output: Nash equilibrium point $f^*\left(i,j\right)$ and mean field $m^*\left(i,j\right)$;

```
for i =1 : X do
    for j =1 : Y+1 do
        if j =Y+1 then
            if f(i,j) =0 then
                m(i+1,j)_temp = m(i,j);
            else
                m(i+1,j)_temp = 0;
            end if
        else
            Calculate m(i+1,j) from Equation (21), let m(i+1,j)_temp = m(i+1,j);
        end if
        if m(i+1,j)_temp > 0 then
            m(i+1,j) = m(i+1,j)_temp;
        else
            m(i+1,j) = 0;
        end if
    end for
end for
for any i, normalize m(i,j) do;
    for i =X+1 : -1 : 1 do
        for j =1 : Y+1 do
            According to Equation (29), get V(i-1,j);
        end for
    end for
    for i =X+1 : -1 : 1 do
        for j =1 : Y+1 do
            According to Equation (29), find the optimal f(i,j);
        end for
    end for
end for
```

Therefore, $m(t,e)$ and $V\left(t,e\right)$ can be transformed into $m\left(i,j\right)$ and $V\left(i,j\right)$, where i and j are the i^{th} point in time space and the j^{th} point in state space. The numerical solution of the FPK equation can be solved by the Lax-Friedrichs method [44]. By using the Lax-Friedrichs method, $m(i+1,j)$ can be expressed in (26). $f\left(i,j\right)$ and $m\left(i,j\right)$ are the sampling frequency and mean field at time i when the remaining energy is j. The derivation in the HJB equation can be approximated by the finite difference method, and $\frac{\partial V(t,e)}{\partial t}$ in the HJB equation can be expressed as

$$\frac{\partial V(t,e)}{\partial t}=\frac{V(i,j)-V(i-1,j)}{\delta}. \tag{27}$$

$\frac{\partial V(t,e)}{\partial e}$ can be expressed as

$$\frac{\partial V(t,e)}{\partial e}=\frac{V(i,j+1)-V(i,j-1)}{2\delta_e}. \tag{28}$$

$$U_m^{mean}\left(f_m\left(t,e_m\right),m\left(t,e\right)\right) = a_1 T_u w_m \frac{Pd_m(f_m(t,e_m))\int_{w>0}\int_{r_m^u>0} e^{-\frac{(e^w-1)\sigma_n^2 (r_m^u)^{-\alpha}}{p_m^u}} 2\pi\lambda_u r_m^u e^{-\pi\lambda_u (r_m^u)^2} dr_m^u dw}{Pd_m(f_m(t,e_m))+(M-1)E^{mean}[Pd_j(f_j(t,e_j))]} - a_2 p_m^s f_m\left(t,e_m\right)\delta \tag{19}$$

.

$$m(i+1,j) = \frac{1}{2}[m(i,j-1)+m(i,j+1)] + p^s[f(i,j+1)m(i,j+1) - f(i,j-1)m(i,j-1)]\frac{\delta}{2(\delta_e)}. \tag{26}$$

$$\frac{V(i,j)-V(i-1,j)}{\delta} + \max_{f(i,j)}(U^{mean}(f\left(i,j\right),m\left(i,j\right)) - p^s f\left(i,j\right)\frac{V(i,j+1)-V(i,j-1)}{2\delta_e}) = 0 \tag{29}$$

Thus, the HJB equation after the finite difference method of approximation is given in (29).

In this paper, the algorithm 1 is proposed to calculate the Nash equilibrium point of the mean field game. Based on the algorithm 1, the Nash equilibrium point f^* and the mean field distribution m^* under the Nash equilibrium point can be obtained.

VI. Network Sensing Fusion Mechanism

A. Mechanism of Local Sensing Fusion Based on AoI

As can be seen from the previous section, the MD m will obtain the optimal sensing strategy $f_m^*\left(t\right)$ according to its utility function at different time slots in the sensing stage. After each MD conducts spectrum sensing according to the optimal sensing strategy, the sensing results will be sent to the smart contract in the form of transactions for the fusion of sensing results. Considering the influence of the dynamic change of PUs state and the difference of sensing data in different time slots on the overall decision results, a two-step mechanism of spectrum sensing fusion based on AoI and CW is proposed in this paper. In this section, the first step of fusion, namely the mechanism of local spectrum sensing fusion based on AoI, is introduced. In the sensing stage, the state of PU will change over time. Thus, the current result of energy detection can better reflect the real state of PU's occupation of the authorized channel than the previous result of energy detection. In the previous section, we discretize the sensing time T_s into X sensing time slots δ, and calculate the optimal sampling frequency of MDs under each sensing time slot δ. Based on this, the sensing number of m in the perception stage N times, that is, $N{=}X$. The sampling frequency of the $i^{th}\left(i=1,2,\cdots,N\right)$ sensing of m is $f_m^*\left(i\right)$, the total sampling number of the i^{th} sensing is $M_m\left(i\right)=f_m^*\left(i\right)\delta{=}\ f_m^*\left(i\right)\frac{T_s}{X}$, and the time of the i^{th} sensing is $tx_m\left(i\right)$.

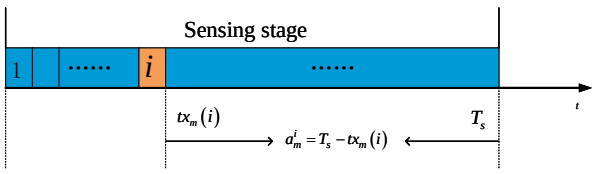

Fig. 4: AoI of local spectrum sensing data.

As shown in Fig. 4, AoI of the sensing data in the i^{th} sensing is defined as the time a_m^i from the end of the current sensing $tx_m\left(i\right)$ to the end of the whole sensing stage T_s, and a_m^i is expressed as $a_m^i = T_s - tx_m\left(i\right)$. The spectrum sensing result with lower value of a_m^i is more accurate than that with higher value of a_m^i, which means that the sensing results with lower value of a_m^i is more important for the local fusion result. So we propose a weight indicator to measure the importance of sensing results obtained during different time slot in the local fusion. The weight $w_{1,m}^i$ of the sensing data of MDs i^{th} sensing in local fusion is expressed as

$$w_{1,m}^i = \frac{\left(a_m^i\right)^{-\beta}}{\sum_{j=1}^{N}\left(a_m^j\right)^{-\beta}}, \tag{30}$$

where β is a constant value. Thus, the local fusion sensing result of m is given by

$$y_m^{tot} = \sum_{i=1}^{N} w_{1,m}^i y_m\left(i\right), \tag{31}$$

where $y_m\left(i\right)$ is the sensing data of the i^{th} sensing of m. When the sampling number of the i^{th} sensing is $f_m\left(i\right)$, $y_m\left(i\right)$ is expressed as

$$y_m\left(i\right) = \frac{1}{f_m\left(i\right)}\sum_{l=1}^{f_m(i)} y_{m,i}\left(l\right), \tag{32}$$

where $y_{m,i}\left(l\right)$ is the sample data of the $l^{th}\left(l=1,2\cdots f_m\left(i\right)\right)$ sampling of the i^{th} sensing. In this paper, we assume that the state of PU changes dynamically in different sensing time slots in the whole sensing time T_s, and the state of PU remains unchanged in the same sensing time slot δ. According to reference [44], $y_m\left(i\right)$ is approximately a Gaussian distribution, and its mean value and variance are as follows

$$H_0\begin{cases}\mu_{m,i}:\sigma_n^2\\ \sigma_{m,i}^2:\frac{2\sigma_n^4}{f_m(i)}\end{cases}\quad H_1\begin{cases}\mu_{m,i}:(\gamma_m+1)\sigma_n^2\\ \sigma_{m,i}^2:\frac{2(2\gamma_m+1)\sigma_n^4}{f_m(i)}\end{cases} \tag{33}$$

H_0 is the frequency band not occupied by PU, H_1 is the frequency band occupied by PU. SNR in the spectrum sensing of m is denoted as γ_m.

To evaluate the performance of AoI-based local sensing data fusion mechanism, we deduce the local sensing detection probability Pd_m^{local} and false alarm probability Pf_m^{local} of m under this mechanism.

Theorem 2: The local sensing detection probability Pd_m^{local} of the proposed fusion mechanism is expressed as

$$Pd_m^{local} = P\left(y_m^{tot} > \lambda \,|H_1\right) = Q\left(\frac{\lambda - E\left[y_m^{tot}|\,H_1\right]}{\sqrt{D\left[y_m^{tot}|\,H_1\right]}}\right), \quad (34)$$

where $E\left[y_m^{tot}|\,H_1\right]$ and $D\left[y_m^{tot}|\,H_1\right]$ are respectively the mean and variance of y_m^{tot} when the final state of PU at the end of sensing is H_1. λ the threshold of sensing result.

Proof: See Appendix B.

Next, the local sensing false alarm probability Pf_m^{local} of m is derived in the same way.

Theorem 3: The local sensing false alarm probability Pf_m^{local} of the proposed fusion mechanism is expressed as

$$Pf_m^{local} = P\left(y_m^{tot} > \lambda \,|H_0\right) = Q\left(\frac{\lambda - E\left[y_m^{tot}|\,H_0\right]}{\sqrt{D\left[y_m^{tot}|\,H_0\right]}}\right). \quad (35)$$

Proof: See Appendix C.

To verify the correctness of the derived Pd_m^{local}, we carry out numerical simulation analysis. According to the proposed local sensing fusion mechanism based on AoI, 1 million times of fusion sensing data are generated in this paper. The detection probabilities under numerical simulation are obtained by comparing the fusion sensing data of 1 million times with the detection threshold λ. As shown in Fig. 5, we obtained the variation curve of Pd_m^{local} with SNR in the theoretical derivation and numerical simulation. We can see from Fig. 5 that the theoretical value Pd_m^{local} is basically consistent with the simulation value, which further verifies the correctness of our derivation process.

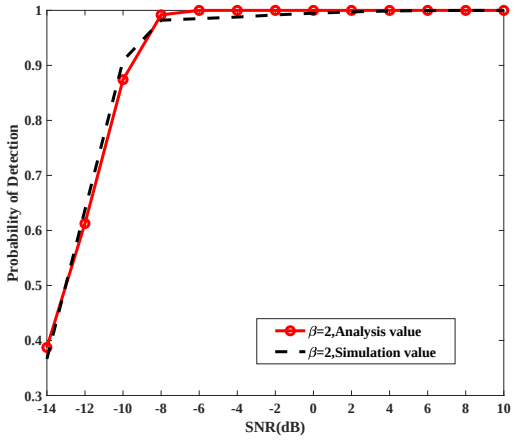

Fig. 5: Local sensing detection probability Pd_m^{local} changes with SNR in theory and numerical simulation.

B. Global Sensing Fusion Mechanism Based on Transaction Cumulative Weight

After the end of the sensing stage T_s, m sends a transaction containing the local fusion sensing data y_m^{tot} to Tangle network and enters the consensus stage T_c. Assuming that the CW value of the transaction issued by m after the end of the consensus stage T_c is denoted as cw_m. The second step of the fusion mechanism proposed in this paper is the global sensing fusion mechanism based on the transaction CW. In this case, the weight $w_{2,m}$ of m's local sensing data in the global sensing fusion result is expressed as

$$w_{2,m} = \frac{cw_m}{\sum_{j=1}^{M} cw_j}. \quad (36)$$

The global sensing fusion result Y^{tot} is expressed as

$$Y^{tot} = \sum_{i=1}^{M} w_{2,i} y_i^{tot}. \quad (37)$$

The MD m issues a transaction at the beginning of the consensus stage. Assuming that the transaction's initial weight is 1. Then based on [14] [45], the growth of the mean value of this transactions CW cw_m is expressed as

$$E\left[cw_m\right] = \begin{cases} 2\exp(\frac{0.352t}{h}), 0 \le t \le t_0 \\ \frac{L}{0.704} + \lambda\left(t - t_0\right), t > t_0, \end{cases} \quad (38)$$

where the time elapsed since the transaction was issued is denoted as t, the CW at time t is denoted as $cw_m\left(t\right)$, the time it takes for a transaction to be received across the network is denoted as h, the rate at which transactions arrive in Tangle Network is denoted as λ, the number of tips expected in Tangle network is expressed as $L = 2\lambda h$, the time dividing point of cw_m is expressed as $t_0 = \frac{h}{0.352}\ln\left(\frac{L}{1.408}\right)$.

To get the distribution characteristics of CW values of different transactions at the same time t, we simulate the propagation mode of transactions in Tangle network and design a growth algorithm 2 for transaction CW values at different times.

The totally time sampling points is denoted as t_num, the CW of tips transaction is denoted as $tips.weight$, generation time of tips transaction is denoted as $tips.time$, current time is denoted as now, the number of current tips transactions is denoted as $size\left(\text{tips}\right)$, generating a random number in the range of $1 \sim$ size is denoted as $random\left(size\right)$, the two transactions referenced by the newly generated tips transaction are denoted as $new\_tx.pre1$ and $new\_tx.pre2$, generation time of the new transaction is denoted as $new\_tx.time$.

In this paper, the algorithm 2 is repeated for 10000 times to simulate the growth and change of transaction CW and its distribution curve at different time, and compares with the theoretical derivation value of Equation (38). The simulation results are shown in Fig. 6. As can be seen from Fig. 6 (a), the average value of transaction CW derived from (38) is basically consistent with the simulated value of CW obtained from algorithm 2 proposed in this paper, thus verifying the effectiveness of algorithm 2 proposed in this paper. It can be seen from Fig. 6 (b) that the CWs of all transactions issued at the same time approximately follow the Poisson distribution. Thus, the algorithm 2 can be used to effectively simulate the growth process of CW of transactions issued by all MDs including local fused perception data y_m^{tot} at the beginning of the consensus stage T_c, so as to get a set of data subject to Poisson distribution to approximately represent

Algorithm 2 Transaction CW growth algorithm in Tangle network

Input: Initialize h, L, $lamda$, t_num;

Output: The transaction CW value at different times in Tangle network;

1: Generate L tips transactions, let $tips.weight = 1$, $tips.time = now$
2: **for** $i = 1 : t\_num$ **do**
3: Generate a random number λ_{rand} following the Poisson distribution of λ, and generate λ_{rand} new transactions new_tx;
4: $size = size\,(tips)$;
5: **if** $size > 2$ **then**
6: $ran1 = random\,(size)$, $ran2 = random\,(size)$;
7: **if** $(ran1 \neq ran2)$ **then**
8: $new\_tx.pre1 = tips\,(ran1)$, $new\_tx.pre2 = tips\,(ran1)$;
9: **end if**
10: **end if**
11: Traverse all new transactions, when $now - new\_tx.time > h$, the transaction is added to the tips queue, while the two transactions $new\_tx.pre1$ and $new\_tx.pre2$ are removed from the tips queue;
12: Traverse all new transactions and look backwards, increasing the weight of all transactions directly and indirectly referenced by that transaction by 1;
13: **end for**

CW of transactions issued by different MES at the end of the consensus stage T_c. By substituting this set of CW data values into (36), we can get the weight $w_{2,m}$ of m in global spectrum sensing fusion. According to the expressions of the mean value and variance of m's local sensing fusion result y_m^{tot} derived in the previous section, in this section, when PU is in the state of H_1, the expectation $e\_global_{H_1}$ of global fusion sensing data Y^{tot} is show as

$$e\_global_{H_1} = \sum_{i=1}^{M} w_{2,i} E\left[y_i^{tot} \middle| H_1\right]. \tag{39}$$

The variance $d\_global_{H_1}$ of global fusion sensing data Y^{tot} is show as in (40).

Similarly, when PU is in the state of H_0, the expectation $e\_global_{H_0}$ of global fusion sensing data Y^{tot} is expressed as

$$e\_global_{H_0} = \sum_{i=1}^{M} w_{2,i} E\left[y_i^{tot} \middle| H_0\right]. \tag{41}$$

The variance $d\_global_{H_0}$ of global fusion sensing data Y^{tot} is expressed in (42). Thus, when the sensing fusion mechanism based on AoI and transaction CW is adopted, the expressions of global detection probability Pd^{Global} and global false alarm probability Pf^{Global} under network CSS architecture are respectively shown as

$$Pd^{Global} = Q\left(\frac{\lambda_1 - e\_global_{H_1}}{\sqrt{d\_global_{H_1}}}\right). \tag{43}$$

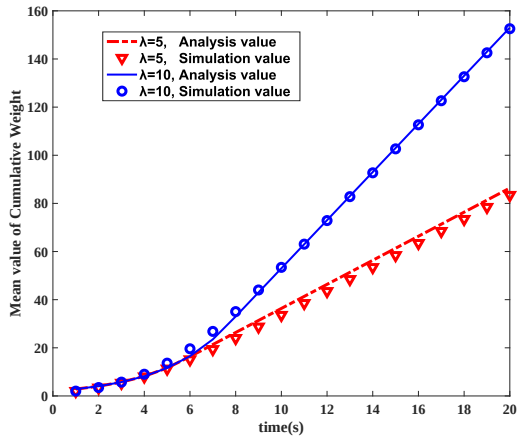

(a) The mean value of CW over time.

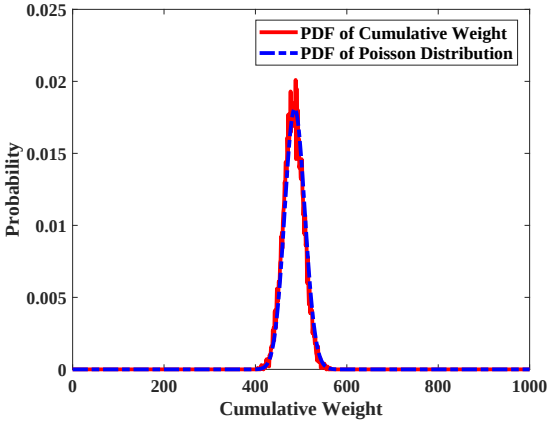

(b) The probability distribution curve of CW.

Fig. 6: The mean value and probability distribution of CW.

$$Pf^{Global} = Q\left(\frac{\lambda_1 - e\_global_{H_0}}{\sqrt{d\_global_{H_0}}}\right). \tag{44}$$

.

C. Signaling Overhead of the Tangle-Based Spectrum Sensing and Fusion Mechanism

The signaling overhead is evaluated by the number of message interactions in the proposed tangle-based networks. Before the spectrum sensing, the PU needs to publish the smart contract to tangle networks, which defines some basic rules about spectrum allocation. Such transactions need to be transmitted to all MDs, so the number of interactions between the PU and MDs is M. When MDs get their optimal spectrum sensing strategy, MDs need to send transactions containing the spectrum sensing strategy to tangle networks, which need to be known by other MDs and PU. We assume that every MD relays any recent transaction data to all its neighbors by the device-to-device communication. The number of message interactions required to synchronize the transaction data to all MDs and PU is $O\,(M \log M)$. Then, each MU can obtain its own available access time of specific frequency band based on the smart contract and other MUs spectrum sensing strategies.

$$
\begin{aligned}
d\_global_{H_1} &= \sum_{i=1}^{M} (w_{2,i})^2 E\left[(y_i^{tot})^2\right] + 2(E\left[y_m^{tot}|\, H_1\right])^2 \sum_{i=1}^{M-1}\left(w_{2,i}\sum_{j=i}^{M} w_{2,j}\right) - (e\_global_{H_1})^2 \\
&= \sum_{i=1}^{M} (w_{2,i})^2 \left(D\left[y_m^{tot}|\, H_1\right] + (E\left[y_m^{tot}|\, H_1\right])^2\right) + 2(E\left[y_m^{tot}|\, H_1\right])^2 \sum_{i=1}^{M-1}\left(w_{2,i}\sum_{j=i}^{M} w_{2,j}\right) - (e\_global_{H_1})^2
\end{aligned} \tag{40}
$$

$$
\begin{aligned}
d\_global_{H_0} &= \sum_{i=1}^{M} (w_{2,i})^2 E\left[(y_i^{tot})^2\right] + 2(E\left[y_m^{tot}|\, H_0\right])^2 \sum_{i=1}^{M-1}\left(w_{2,i}\sum_{j=i}^{M} w_{2,j}\right) - (e\_global_{H_0})^2 \\
&= \sum_{i=1}^{M} (w_{2,i})^2 \left(D\left[y_m^{tot}|\, H_0\right] + (E\left[y_m^{tot}|\, H_0\right])^2\right) + 2(E\left[y_m^{tot}|\, H_0\right])^2 \sum_{i=1}^{M-1}\left(w_{2,i}\sum_{j=i}^{M} w_{2,j}\right) - (e\_global_{H_0})^2.
\end{aligned} \tag{42}
$$

So the overall interaction caused in the tangle transaction is $M + O(M \log M)$.

VII. Performance analysis

In this section, the performance simulation is carried out for the optimization of the sensing strategy based on the mean field game and the spectrum sensing fusion mechanism based on AoI and transaction CW proposed in this paper. The related parameters are shown in Table 1 [14] [46].

TABLE I: Parameter settings

Parameter	Value
Maximum sensing energy of MD $E_{\max}$	2J
Path loss exponent α	3
Interference noise σ_n^2	10^{-8}
Time T_s	1s
Average SNR $\overline{\gamma}$	5dB
The total number of time points X	51
The total number of state points Y	51
Parameter β	2,3
Detection threshold λ_1	24
Time for a transaction to be received by the network h	0.1
The rate at which transactions arrive in Tangle network λ	5,10

For intuitive analysis, the optimal sampling frequency f^* of MDs in different time slots by time slot δ is multiplied to get the optimal sensing sampling times of MDs in different time slots. Fig. 7 shows the change of the optimal sensing sampling times of MDs with time and remaining energy of MDs. It can be seen from Fig. 7 that with the increase of time and the decrease of remaining energy of MDs, the optimal sensing sampling times of MDs also decrease. To more intuitively display the simulation results in Fig. 7, the variation of the sampling size of MD with the remaining energy state of MDs at three different times of 0s, 0.5s and 1s are shown in Fig. 8(a). It can be seen from Fig 8(a) that under the same remaining energy, the sampling size of MDs decreases with the increase of time. At the same time, the sampling size of MDs increases with the increase of the remaining energy. This is because when the remaining energy of MDs is large, there is enough energy to increase the sampling number of MDs. Meanwhile, Fig. 8(b) shows the change curve of sampling size of MDs with time under three different remaining energy states 0J, 1J and 2J. It can be seen from Fig. 8(b) that the changes of sampling sizes of MDs with time and remaining energy state are consistent with that of Fig. 8(a).

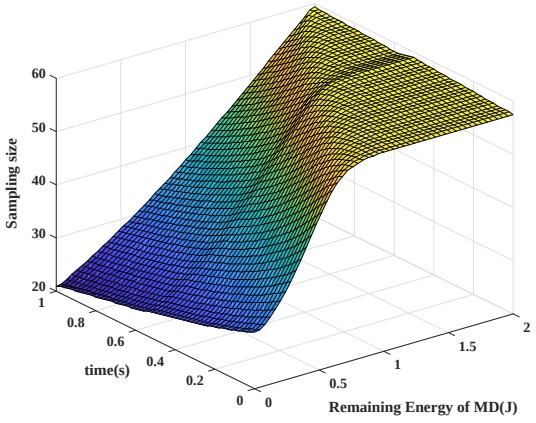

Fig. 7: Control strategy of sensing sampling times of MD.

Fig. 9 shows the variation curve of mean field with time and the remaining energy of MDs. As can be seen from Fig. 9, as time increases, the proportion of MDs in the state of low remaining energy becomes smaller and smaller. To explain the simulation results in Fig. 9 more intuitively, the change of MF with the remaining energy of MD at three different time of 0s, 0.5s and 1s, and the change of MF with time at three different states of 0J, 1J and 2J are shown in Fig. 10. As can be seen from Fig. 10 (a), as time goes by, the proportion of MDs in the state of low remaining energy keeps increasing, while the proportion of MDs in the state of high remaining energy gradually decreases. This is because as time goes by, MDs keep sampling and consuming energy, and MDs in the state of high remaining energy gradually decrease. When the remaining energy of MD is around 0.6 J, the proportion of MDs with $t = 0s$ and those with $t = 1s$ are the same. Similarly, when the remaining energy of MD is around 1.2 J, the proportion of MDs with $t = 0s$ and those with $t = 0.5s$ are the same. As can be seen from Fig. 10 (b), when the time is fixed, the proportion of MDs with remaining energy of 0J is higher than that of MDs with remaining energy of 1J and 2J. The proportion of MDs with remainign energy of 0J increases with the increase of time, because the remaining energy of MDs is constantly exhausted with the increase of time. The proportion of MDs with the remaining energy of 1J

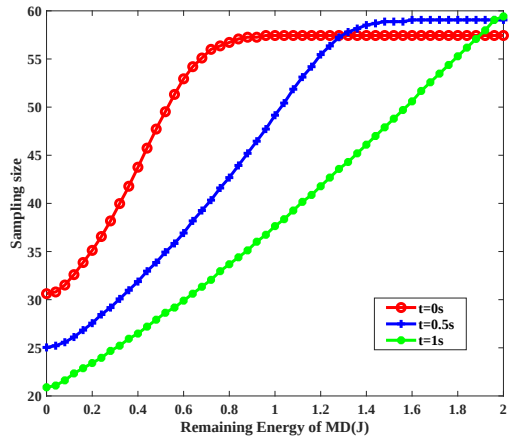

(a) Sampling size changes with remaining energy of MD.

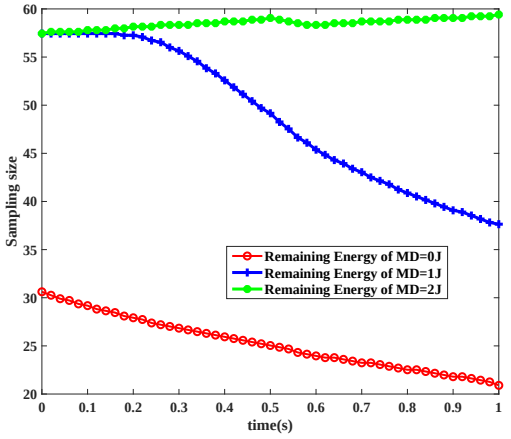

(b) Sampling size changes with time.

Fig. 8: Sensing sampling times of MD.

increases first and then decreases with the increase of time. This is because, as shown in Fig. 8 (b), the sampling times of MDs with the remaining energy of 1J is at a relatively high value. When the time is less than 0.7s, MDs with remaining energy greater than 1J keep a high sampling frequency and constantly consume energy, so that the proportion of MDs with remaining energy of 1J increases. When the time is greater than 0.7s, the proportion of MDs with the remaining energy of 1J begins to decrease gradually, thus forming a change trend of increasing first and then decreasing. For MDs with a remaining energy of 2J, since all MDs consume energy through sensing sampling and the initial residual energy of MDs is 2J, as time increases, the proportion of MDs with a remaining energy of 2J will decrease sharply until it reaches 0.

In order to better reflect the effectiveness of the variable sensing sampling strategy proposed in this paper, the overall weighted sensing utility under the mechanism proposed in this paper is compared with the value of the fixed sensing sampling strategy at a certain moment. At time $i\,(i=1,2,\cdots,X)$, the overall weighted utility $\overline{U_{tol,i}}$ of the network is expressed as the weighted value of the sensing utility of MD in different

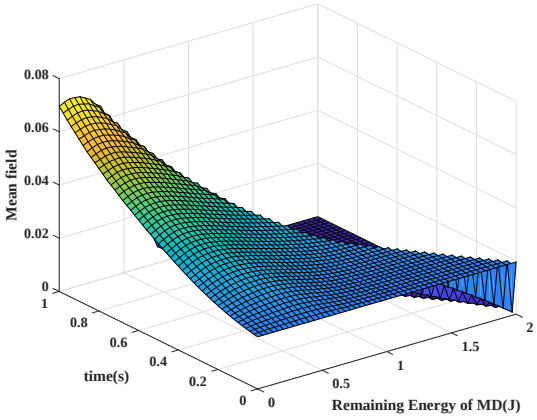

Fig. 9: Distribution of mean field.

states is shown as

$$\overline{U_{tol,i}}=\sum_{j}U^{mean}\left(i,j\right)m^{*}\left(i,j\right). \tag{45}$$

It is assumed that the sampling times of the fixed sensing sampling strategy is $f_{\max}$, and the simulation results are shown in Fig. 11. As can be seen from Fig. 11, when the variable sensing sampling strategy proposed in this paper is adopted, the overall weighted sensing utility of the network basically remains stable. Compared with the fixed sensing sampling strategy, the weighted sensing utility of the proposed strategy is increased by 10% on average. Moreover, the weighted sensing utility of the strategy proposed in this paper is always higher than that of the fixed strategy in the whole time period, which indicates that the dynamically regulated sensing sampling strategy proposed in this paper can maintain good sensing utility even when large-scale MDs is in a state of low remaining energy as a whole.

In this paper, the weighted sensing detection probability of network $\overline{Pd_{net\_tol}}$ is used as a performance index to compare and analyze the performance differences between the dynamic regulation sensing sampling strategy proposed in this paper and the fixed sensing sampling strategy. The weighted sensing detection probability of network $\overline{Pd_{net\_tol}}$ is the weighted sum of detection probabilities of MEs in different states at time $i\,(i=1,2,\cdots,X)$ is

$$\overline{Pd_{net\_tol}}=\sum_{j}m^{*}\left(i,j\right)Pd\left(i,j\right), \tag{46}$$

where the detection probability under the condition that the sampling strategy is the optimal strategy solution $f^{*}\left(i,j\right)$ at time i and j is denoted as $Pd\left(i,j\right)$.

Fig. 12 shows the simulation results of $\overline{Pd_{net\_tol}}$ under different values of $\overline{\gamma}$. It can be seen from Fig. 12 that $\overline{Pd_{net\_tol}}$ of the sensing sampling strategy proposed in this paper is basically stable in the whole sensing period. At the initial time, $\overline{Pd_{net\_tol}}$ of the strategy proposed in this paper is less than that of the fixed strategy. However, with the increase of time, $\overline{Pd_{net\_tol}}$ of the strategy proposed in this paper will be better

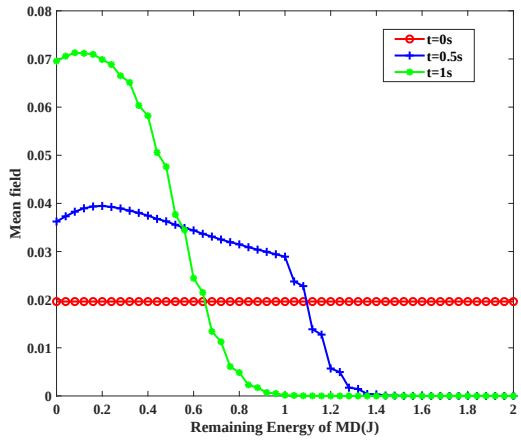

(a) Mean field changes with remaining energy of MD.

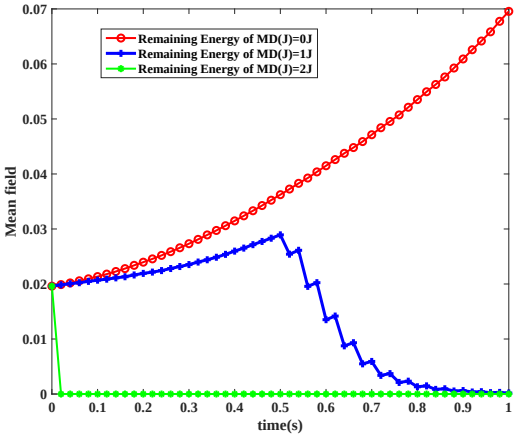

(b) Mean field changes with time.

Fig. 10: Mean field of MD.

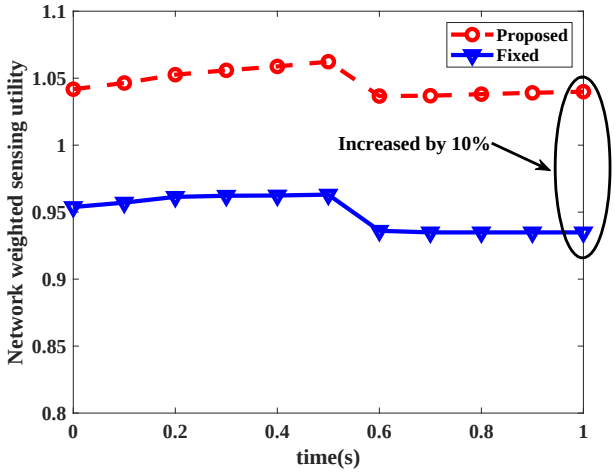

Fig. 11: Performance of network weighted utility over time.

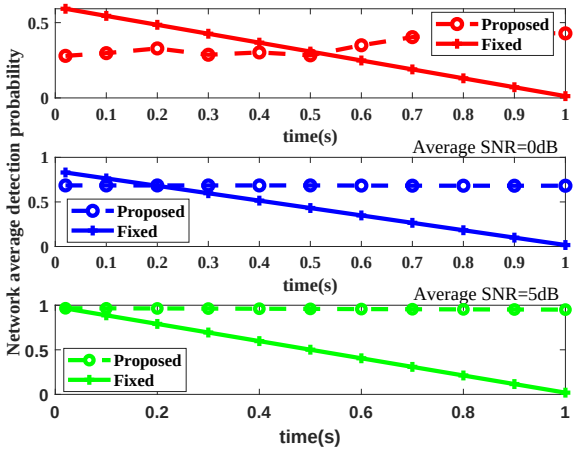

Fig. 12: Network average sensing detection probability performance over time.

than that of the fixed strategy when $\overline{\gamma}$ corresponds to -5dB, 0dB and 5dB, and the time corresponds to 0.5s, 0.2s and 0s.

To evaluate the performance of the proposed spectrum sensing fusion mechanism based on AoI and transaction CW, the performance of the local spectrum sensing fusion mechanism based on AoI was simulated. Fig. 13 shows the variation curve of local detection probability with SNR and false alarm probability. Fig. 13(a) shows the variation curve of local detection probability with SNR. It can be seen from Fig. 13 (a) that the local detection probability increases with the increase of SNR. When SNR is -10dB, compared with the equal-weight fusion mechanism, the AoI-based local sensing fusion mechanism proposed in this paper has the largest percentage improvement of detection probability, which is 42.13%. Fig. 13 (b) shows the relationship curve between local detection probability and false alarm probability, and the SNR at this time is set to -10dB. It can be seen from Fig. 13 (b) that the local detection probability increases with the increase of false alarm probability. Under the same false alarm probability, the detection probability of AoI-based local sensing fusion mechanism proposed in this paper is higher than that of the equal-weight fusion method.

Fig. 14 shows the variation curve of local false alarm probability and local error probability with SNR. It can be seen from Fig. 14 (a) that the local false alarm probability decreases with the increase of SNR and β. When SNR is -6dB, the false alarm probability of AoI-based local sensing fusion mechanism almost drops to 0, while the false alarm probability of the equal-weight fusion method is 0.2097. The false alarm probability of AoI-based local sensing fusion mechanism proposed in this paper is 99.61% lower than that of the equal-weight mechanism. Fig. 14 (b) shows that the local error probability decreases with the increase of SNR, where the local error probability is defined as $Pe_m^{local} = 1-Pd_m^{local}+Pf_m^{local}$. As can be seen from the fig. 14 (b), under the same SNR values, the overall error probability of AoI-based local fusion mechanism proposed in this paper is less than that of equal-weight fusion mechanism. This is because when considering the state of the PU dynamic variable, the closer to the end of the sensing of sensing data will be closer to the real state of PU. When local fusion based on AoI is

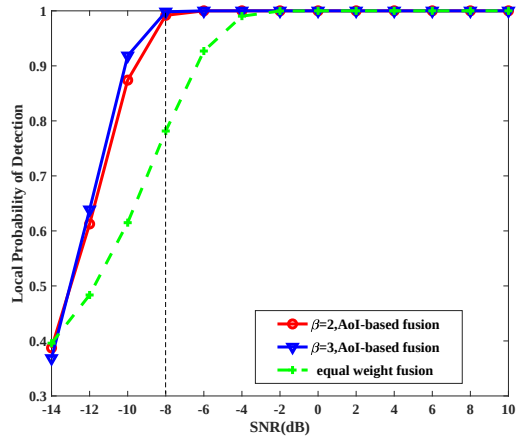

(a) Local detection probability changes with SNR.

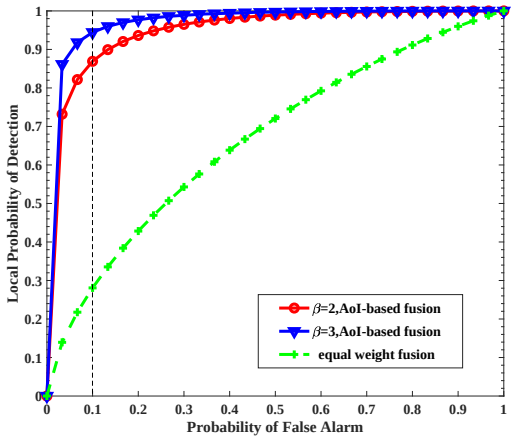

(b) Local detection probability changes with false alarm probability

Fig. 13: Local detection probability of MD.

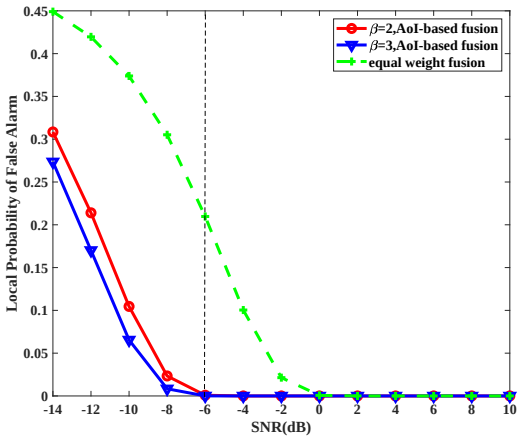

(a) Local false alarm probability varies with SNR.

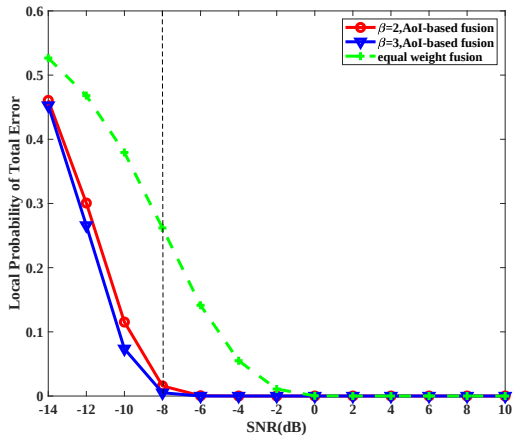

(b) Local error probability varies with SNR.

Fig. 14: Local false alarm probability and Local error probability.

adopted, the final result of global sensing fusion will be more accurate, and the overall error probability will be smaller.

Fig. 15 shows the global detection probability of the two-step spectrum sensing fusion mechanism based on AoI and transaction CW changes with the mean of SNR and false alarm probability. The distance between PU and MDs follows the Poisson distribution. When given transmit power and noise level, we can obtain the probability distribution function of SNR [47]. The proposed fusion mechanism is compared with traditional Maximal Ratio Combining (MRC), Selection Combing (SC) and Square-Law Selection (SLS). In MRC, each signal branch is multiplied by a weight factor that is proportional to the signal amplitude. The SC scheme is a soft fusion scheme that directly selects the branch with the maximum SNR in the selection combiner. The SLS scheme only selects the branch with the largest remaining energy. It can be seen from Fig. 15 (a) that under the same mean of SNR, the global detection probability of the sensing fusion mechanism proposed in this paper is higher than that of the traditional MRC, SC and SLS mechanism. When SNR is -8dB, the global detection probability of the two-step sensing fusion mechanism proposed in this paper is 1, and the detection probability of the MRC, SLS and SC mechanism are 0.4513, 0.2764 and 0.003, respectively. Fig. 15 (b) shows the change of global detection probability with false alarm probability. It can be seen from Fig. 15 (b) that global detection probability increases with the increase of false alarm probability. Compared with the traditional MRC mechanism, the proposed two-step spectrum sensing fusion mechanism based on AoI and transaction CW has the highest global detection probability improved by 30.23%.

Fig. 16 (a) shows the change of global false alarm probability with mean of SNR. As can be seen from Fig. 16 (a), under the same average SNR, the global false alarm probability of the sensing fusion mechanism proposed in this paper is lower than that of the traditional MRC, SC and SLS mechanism. mechanism. C Fig. 16 (b) shows the change of global error probability with SNR. As can be seen from Fig. 16 (b), the global error probability of the sensing fusion mechanism proposed in this paper is smaller than that of the MRC mechanism under the same average SNR. When the mean of SNR is -14dB, the global error probability of the proposed two-step sensing fusion mechanism is 21.8% lower

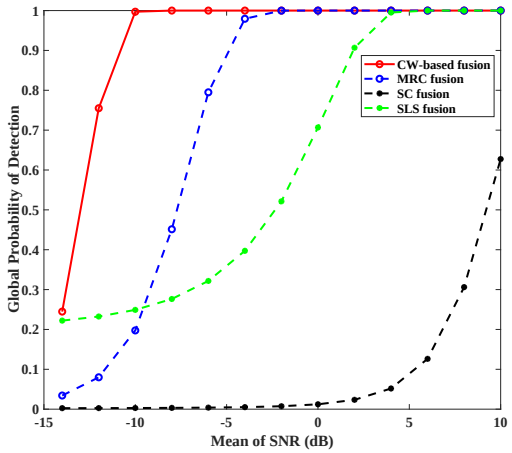

(a) Global detection probability changes with mean of SNR.

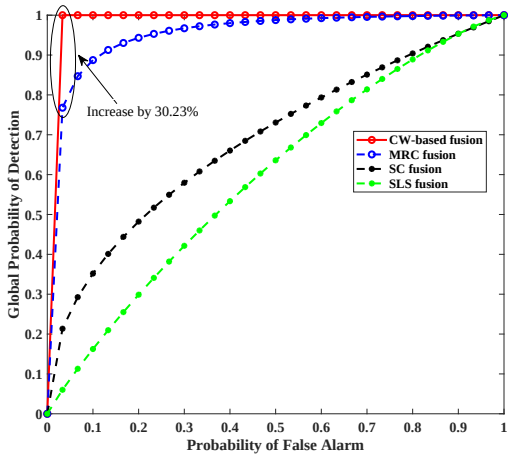

(b) Global detection probability changes with false alarm probability.

Fig. 15: Global detection probability.

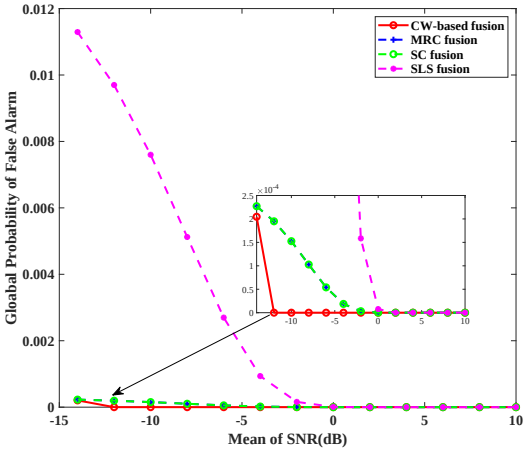

(a) Global false alarm probability varies with SNR.

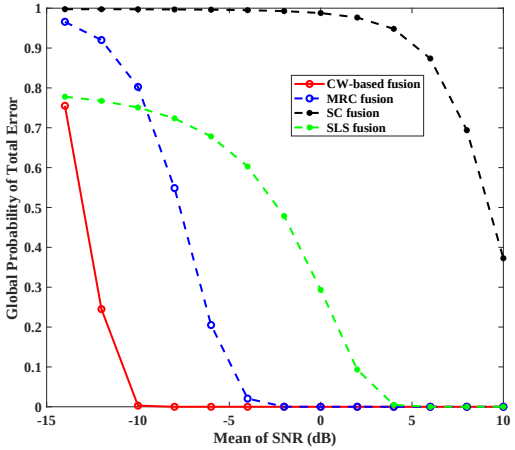

(b) Global error probability varies with mean of SNR.

Fig. 16: Global false alarm probability and global error probability.

than that of the MRC mechanism.

VIII. Conclusion

In this paper, the CSS architecture based on Tangle blockchain is constructed. Massive MDs act as spectrum sensing nodes and blockchain nodes, and the spectrum sensing results are sent to the smart contract in the form of transactions without the introduction of traditional fusion center. Considering the energy limitation of massive MDs in the CSS and the optimization demand of sensing utilization, a novel algorithm that can improve the spectrum sensing results of massive MDs in dynamic environment has been proposed based on the mean field game. We also propose a new two-step spectrum sensing fusion mechanism based on the AoI and CW of transactions to address the impact of perceptual data differences in different time slots on the overall decision. The simulation results show that, compared with the traditional fixed spectrum sensing strategy, the proposed dynamic spectrum sensing strategy can improve the sensing utility of massive MDs when the residual energy is low, and the weighted sensing utility of massive MDs is improved by 10% on average. Moreover, compared to the traditional soft fusion mechanism, the detection probability of the proposed two-step spectrum sensing fusion mechanism based on the AoI and CW is maximally increased by 30.23%, and the false alarm probability is minimally reduced by 9.92%.

Appendix A
Proof of Theorem 1

The Nash equilibrium solution of stochastic differential game can be obtained by solving the above HJB equation [41]. Thus, the existence of Nash equilibrium can be proved by proving that Equation (12) is solvable.

According to reference [43], the Hamiltonian equation related to Equation (12) is expressed as

$$H\left(e_m, \frac{\partial V_m(t,e_m(t))}{\partial e}\right) = \max_{f_m(t,e_m)} \left[U_m\left(f_m\left(t,e_m\right)\right) - p_m^s f_m\left(t,e_m\right) \frac{\partial V_m(t,e_m(t))}{\partial e}\right]. \tag{47}$$

Equation (12) is solvable only if Equation (47) is solvable, and Equation (47) is solvable only if Hamiltonian is smooth.

$$H\left(e_m, \frac{\partial V_m\left(t,e_m\left(t\right)\right)}{\partial e}\right) = \max_{f_m(te_m)} \left[a_1 T_u \frac{Pd_m\left(f_m\left(t,e_m\right)\right)}{\sum_{j=1}^{M} Pd_j\left(f_j\left(t,e_j\right)\right)} R_m w_m - a_2 p_m^s f_m\left(t,e_m\right)\delta - p_m^s f_m\left(t,e_m\right) \frac{\partial V_m\left(t,e_m\left(t\right)\right)}{\partial e} \right]. \tag{48}$$

$$\begin{aligned} \frac{\partial Pd_m(f_m(t,e_m))}{\partial f_m(t,e_m)} &= \frac{\partial Q\left(\frac{Q^{-1}(Pf_m)-\gamma_m\sqrt{f_m(t,e_m)\delta}}{\sqrt{2\gamma_m+1}}\right)}{\partial f_m(t,e_m)} \\ &= -\frac{1}{\sqrt{2\pi}}\exp\left(-\frac{1}{2}\left(\frac{Q^{-1}(Pf_m)-\gamma_m\sqrt{f_m(t,e_m)\delta}}{\sqrt{2\gamma_m+1}}\right)^2\right)\frac{\partial\left(\frac{Q^{-1}(Pf_m)-\gamma_m\sqrt{f_m(t,e_m)\delta}}{\sqrt{2\gamma_m+1}}\right)}{\partial f_m(t,e_m)} \\ &= \frac{\gamma_m\delta(f_m(t,e_m)\delta)^{-\frac{1}{2}}}{2\sqrt{2\pi(2\gamma_m+1)}}\exp\left(-\frac{\left(Q^{-1}(Pf_m)-\gamma_m\sqrt{f_m(t,e_m)\delta}\right)^2}{2(2\gamma_m+1)}\right). \end{aligned} \tag{49}$$

Substituting Equation (5) into Equation (47) can be obtained as shown in (48). In which the differential variable of Equation (48) is denoted as $f_m\left(t,e_m\right)$. Since $V_m\left(t,e_m\left(t\right)\right)$, R_m and $\sum_{j=1}^{M} Pd_j\left(f_j\left(t,e_j\right)\right)$ are independent of the specific sensing strategies of MD, their derivatives with respect to $f_m\left(t,e_m\right)$ are 0. The derivative of $Pd_m\left(f_m\left(t,e_m\right)\right)$ with respect to $f_m\left(t,e_m\right)$ is expressed in (49). It can be seen from Equation (49) that the first derivative of $Pd_m\left(f_m\left(t,e_m\right)\right)$ with respect to $f_m\left(t,e_m\right)$ exists, and the first derivative is an elementary function, then any derivative of $Pd_m\left(f_m\left(t,e_m\right)\right)$ with respect to $f_m\left(t,e_m\right)$ exists. So any derivative of $H\left(e_m, \frac{\partial V_m(t,e_m)}{\partial e}\right)$ with respect to $f_m\left(t,e_m\right)$ exists, that is, Hamiltonian is smooth for $f_m\left(t,e_m\right)$, and Nash equilibrium solutions for stochastic differential games exists.

APPENDIX B
PROOF OF THEOREM 2

According to the character of the Gaussian distribution, the local fusion sensing result y_m^{tot} of m follows the Gaussian distribution. From the definition of detection probability, the expression of detection probability can be obtained in (34). We next derive the expression for $E\left[y_m^{tot}\middle|H_1\right]$ and $D\left[y_m^{tot}\middle|H_1\right]$.

Considering the dynamic change of PUs state, in this paper, it is assumed that the sensing data of the last $u\,(u=0,1,2,\cdots,N)$ continuous time slots in N sensing time slots is a Gaussian distribution under the condition of H_1, and the value of u is a uniform distribution with probability of $\frac{1}{N+1}$. The sensing data of the $N-u$ time slot follows the Gaussian distribution under the condition of H_0. The probability of the sensing data of the $1\sim(N-u-1)$ time slot following the Gaussian distribution under the condition of H_0 is 1/2, and the probability of following the Gaussian distribution under the condition of H_0 is 1/2. Based on the above hypothesis, the mean value of the sensing data of the last u time slots is expressed as $\sum_{i=N-u+1}^{N} w_{1,m}^i\left(\gamma_m+1\right)\sigma_n^2$, the mean value of the sensing data in the $N-u$ time slot is expressed as $w_{1,m}^{N-u}\sigma_n^2$, the mean value of the sensing data from the 1 to $N-u-1$ time slots is expressed as $\sum_{i=1}^{N-u-1} w_{1,m}^i\left(\frac{1}{2}\left(\gamma_m+1\right)\sigma_n^2+\frac{1}{2}\sigma_n^2\right)$. Thus, when the final state of PU at the end of sensing is H_1, the mean value $E\left[y_m^{tot}\middle|H_1\right]$ of y_m^{tot} is expressed in (50). It can be known from the properties of the variance that

$$D\left[y_m^{tot}\middle|H_1\right] = E\left[\left(y_m^{tot}\right)^2\middle|H_1\right] - E\left[y_m^{tot}\middle|H_1\right]^2, \tag{51}$$

where $E[y_m^{tot}|H_1]^2$ can be calculated according to Equation (52). There are some conditions that we should consider: 1) When $u=N$, that is, the sensing data of all the sensing time slots follow the Gaussian distribution under the condition of H_1. $E\left[\left(y_m^{tot}\right)^2\middle|H_1\right]$ is expressed in (53); 2) When $u=0$, that is the sensing data of the N^{th} time slot follow the Gaussian distribution under the condition of H_0, the sensing data of the $1\sim(N-1)$ time slots have a probability of 1/2 to follow the Gaussian distribution under the condition of H_0, and the probability of 1/2 to follow the Gaussian distribution under the condition of H_1. $E\left[\left(y_m^{tot}\right)^2\middle|H_1\right]$ is expressed in (54); 3) Similarly, when $u\neq 0$ and $u\neq N$, $E\left[\left(y_m^{tot}\right)^2\middle|H_1\right]$ is expressed in (55). Substituting $E\left[\left(y_m^{tot}\right)^2\middle|H_1\right]$ in different cases into Equation (51), the variance $D\left[y_m^{tot}\middle|H_1\right]$ of y_m^{tot} and the expression for Pd_m^{local} can be obtained.

APPENDIX C
PROOF OF THEOREM 3

Similarly, it is assumed that in N sensing time slots, the sensing data of the last $v\,(v=0,1,2,\cdots,N)$ continuous time slots follow the Gaussian distribution under the condition of H_0, and the value of v follows the uniform distribution with a probability of $\frac{1}{N+1}$. Then the sensing data of the $N-v^{th}$ time slot follow the Gaussian distribution under the condition of H_1. In the $1\sim(N-v-1)$ time slots, the probability of the sensing data following the Gaussian distribution under the condition of H_0 is 1/2, and the probability of the sensing data following the Gaussian distribution under the condition of H_1 is 1/2. Similar to the derivation of the mean value in Pd_m^{local}, $E\left[y_m^{tot}\middle|H_0\right]$ is expressed in (56). Similarly, according to $D\left[y_m^{tot}\middle|H_0\right] = E\left[\left(y_m^{tot}\right)^2\middle|H_0\right] - E[y_m^{tot}|H_0]^2$, $E[y_m^{tot}|H_0]^2$ is expressed as: 1) When $v=N$, $E\left[\left(y_m^{tot}\right)^2\middle|H_0\right]$ is expressed in (57); 2) When $v=0$, $E\left[\left(y_m^{tot}\right)^2\middle|H_0\right]$ is expressed in (58); 3) When $v\neq 0$ and

$$E\left[y_m^{tot}\middle|H_1\right]=\frac{1}{N+1}\sum_{u=0}^{N}\left(\sum_{i=1}^{N-u-1}w_{1,m}^{i}\left(\frac{1}{2}\left(\gamma_m+1\right)\sigma_n^2+\frac{1}{2}\sigma_n^2\right)+w_{1,m}^{N-u}\sigma_n^2+\sum_{i=N-u+1}^{N}w_{1,m}^{i}\left(\gamma_m+1\right)\sigma_n^2\right). \tag{50}$$

$$\begin{aligned}E\left[\left(y_m^{tot}\right)^2\middle|H_1\right]&=E\left[\left(w_{1,m}^{1}y_m\left(1\right)+w_{1,m}^{2}y_m\left(2\right)+\cdots+w_{1,m}^{N}y_m\left(N\right)\right)^2\right]\\&=\sum_{i=1}^{N}E\left[\left(w_{1,m}^{i}y_m\left(i\right)\right)^2\right]+2\sum_{i=1}^{N-1}\left(E\left[w_{1,m}^{i}y_m\left(i\right)\right]\sum_{j=i}^{N}E\left[w_{1,m}^{j}y_m\left(j\right)\right]\right).\end{aligned} \tag{52}$$

$$\begin{aligned}E\left[\left(y_m^{tot}\right)^2\middle|H_1\right]&=\sum_{i=1}^{N}\left(w_{1,m}^{i}\right)^2E\left[\left(y_m\left(i\right)\right)^2\right]+2\left(\left(\gamma_m+1\right)\sigma_n^2\right)^2\sum_{i=1}^{N-1}\left(w_{1,m}^{i}\sum_{j=i}^{N}w_{1,m}^{j}\right)\\&=\sum_{i=1}^{N}\left(w_{1,m}^{i}\right)^2\left(D\left[y_m\left(i\right)\right]+E[y_m\left(i\right)]^2\right)+2\left(\left(\gamma_m+1\right)\sigma_n^2\right)^2\sum_{i=1}^{N-1}\left(w_{1,m}^{i}\sum_{j=i}^{N}w_{1,m}^{j}\right)\\&=\sum_{i=1}^{N}\left(w_{1,m}^{i}\right)^2\left(\frac{2(2\gamma_m+1)\sigma_n^4}{f_m(i)}+\left(\left(\gamma_m+1\right)\sigma_n^2\right)^2\right)+2\left(\left(\gamma_m+1\right)\sigma_n^2\right)^2\sum_{i=1}^{N-1}\left(w_{1,m}^{i}\sum_{j=i}^{N}w_{1,m}^{j}\right)\end{aligned}. \tag{53}$$

$$\begin{aligned}E\left[\left(y_m^{tot}\right)^2\middle|H_1\right]=&\tfrac{1}{2}\sum_{i=1}^{N-1}\left(w_{1,m}^{i}\right)^2\left(\tfrac{2(2\gamma_m+1)\sigma_n^4}{f_m(i)}+\left(\left(\gamma_m+1\right)\sigma_n^2\right)^2+\tfrac{2\sigma_n^4}{f_m(i)}+\sigma_n^4\right)+\left(w_{1,m}^{N}\right)^2\left(\tfrac{2\sigma_n^4}{f_m(i)}+\sigma_n^4\right)\\&+\left(\sigma_n^2+\left(\gamma_m+1\right)\sigma_n^2\right)\sum_{i=1}^{N-1}\left(w_{1,m}^{i}\left(\tfrac{1}{2}\left(\sigma_n^2+\left(\gamma_m+1\right)\sigma_n^2\right)\sum_{j=i}^{N-1}w_{1,m}^{j}+\sigma_n^2w_{1,m}^{N}\right)\right).\end{aligned} \tag{54}$$

$$\begin{aligned}E\left[\left(y_m^{tot}\right)^2\middle|H_1\right]=&\tfrac{1}{2}\sum_{i=1}^{N-u-1}\left(w_{1,m}^{i}\right)^2\left(\tfrac{2(2\gamma_m+1)\sigma_n^4}{f_m(i)}+\left(\left(\gamma_m+1\right)\sigma_n^2\right)^2+\tfrac{2\sigma_n^4}{f_m(i)}+\sigma_n^4\right)\\&+\left(w_{1,m}^{N-u}\right)^2\left(\tfrac{2\sigma_n^4}{f_m(i)}+\sigma_n^4\right)+\sum_{j=N-u+1}^{N}\left(w_{1,m}^{j}\right)^2\left(\tfrac{2(2\gamma_m+1)\sigma_n^4}{f_m(j)}+\left(\left(\gamma_m+1\right)\sigma_n^2\right)^2\right)\\&+\left(\sigma_n^2+\left(\gamma_m+1\right)\sigma_n^2\right)\sum_{i=1}^{N-u-1}\left(w_{1,m}^{i}\left(\tfrac{1}{2}\left(\sigma_n^2+\left(\gamma_m+1\right)\sigma_n^2\right)\sum_{j=i+1}^{N-u-1}w_{1,m}^{j}+\sigma_n^2w_{1,m}^{N-u}+\sum_{j=N-u+1}^{N}w_{1,m}^{j}\left(\gamma_m+1\right)\sigma_n^2\right)\right)\\&+2\sigma_n^2\left(\gamma_m+1\right)\sigma_n^2w_{1,m}^{N-u}\sum_{j=N-u+1}^{N}w_{1,m}^{j}+2\left(\left(\gamma_m+1\right)\sigma_n^2\right)^2\sum_{j=N-u+1}^{N-1}w_{1,m}^{j}\sum_{z=j+1}^{N}w_{1,m}^{z}\end{aligned}. \tag{55}$$

$$E\left[y_m^{tot}\middle|H_0\right]=\frac{1}{N+1}\sum_{v=0}^{N}\left(\sum_{i=1}^{N-v-1}w_{1,m}^{i}\left(\frac{1}{2}\left(\gamma_m+1\right)\sigma_n^2+\frac{1}{2}\sigma_n^2\right)+w_{1,m}^{N-v}\left(\gamma_m+1\right)\sigma_n^2+\sum_{i=N-v+1}^{N}w_{1,m}^{i}\sigma_n^2\right). \tag{56}$$

$$E\left[\left(y_m^{tot}\right)^2\middle|H_0\right]=\sum_{i=1}^{N}\left(w_{1,m}^{i}\right)^2\left(\frac{2\sigma_n^4}{f_m\left(i\right)}+\sigma_n^4\right)+2\sigma_n^4\sum_{i=1}^{N-1}\left(w_{1,m}^{i}\sum_{j=i}^{N}w_{1,m}^{j}\right). \tag{57}$$

$$\begin{aligned}E\left[\left(y_m^{tot}\right)^2\middle|H_0\right]=&\tfrac{1}{2}\sum_{i=1}^{N-1}\left(w_{1,m}^{i}\right)^2\left(\tfrac{2(2\gamma_m+1)\sigma_n^4}{f_m(i)}+\left(\left(\gamma_m+1\right)\sigma_n^2\right)^2+\tfrac{2\sigma_n^4}{f_m(i)}+\sigma_n^4\right)\\&+\left(w_{1,m}^{N}\right)^2\left(\tfrac{2(2\gamma_m+1)\sigma_n^4}{f_m(i)}+\left(\left(\gamma_m+1\right)\sigma_n^2\right)^2\right)\\&+\left(\sigma_n^2+\left(\gamma_m+1\right)\sigma_n^2\right)\sum_{i=1}^{N-1}\left(w_{1,m}^{i}\left(\tfrac{1}{2}\left(\sigma_n^2+\left(\gamma_m+1\right)\sigma_n^2\right)\sum_{j=i}^{N-1}w_{1,m}^{j}+\left(\gamma_m+1\right)\sigma_n^2w_{1,m}^{N}\right)\right)\end{aligned}. \tag{58}$$

$v\neq N$, $E\left[\left(y_m^{tot}\right)^2\middle|H_0\right]$ is expressed in (59); From the above derivation of $E\left[\left(y_m^{tot}\right)^2\middle|H_0\right]$ in the different cases, we can get $D\left[y_m^{tot}\middle|H_0\right]$, and finally we can get an expression for Pf_m^{local}.

REFERENCES

[1] X. Ge, B. Yang, J. Ye, G. Mao, C. -X. Wang and T. Han, "Spatial Spectrum and Energy Efficiency of Random Cellular Networks," IEEE Transactions on Communications, vol. 63, no. 3, pp. 1019-1030, March 2015.

$$
\begin{aligned}
&E\left[\left(y_m^{tot}\right)^2\middle| H_0\right] = \tfrac{1}{2}\sum_{i=1}^{N-v-1}\left(w_{1,m}^i\right)^2\left(\tfrac{2(2\gamma_m+1)\sigma_n^4}{f_m(i)}+\left(\left(\gamma_m+1\right)\sigma_n^2\right)^2+\tfrac{2\sigma_n^4}{f_m(i)}+\sigma_n^4\right)\\
&+\left(w_{1,m}^{N-v}\right)^2\left(\tfrac{2(2\gamma_m+1)\sigma_n^4}{f_m(i)}+\left(\left(\gamma_m+1\right)\sigma_n^2\right)^2\right)+\sum_{j=N-v+1}^{N}\left(w_{1,m}^j\right)^2\left(\tfrac{2\sigma_n^4}{f_m(i)}+\sigma_n^4\right)\\
&+\left(\sigma_n^2+\left(\gamma_m+1\right)\sigma_n^2\right)\sum_{i=1}^{N-v-1}\left(w_{1,m}^i\left(\tfrac{1}{2}\left(\sigma_n^2+\left(\gamma_m+1\right)\sigma_n^2\right)\sum_{j=i+1}^{N-v-1}w_{1,m}^j+\left(\gamma_m+1\right)\sigma_n^2 w_{1,m}^{N-v}+\sum_{j=N-v+1}^{N}w_{1,m}^j\sigma_n^2\right)\right)\\
&+2\sigma_n^2\left(\gamma_m+1\right)\sigma_n^2 w_{1,m}^{N-v}\sum_{j=N-v+1}^{N}w_{1,m}^j+2\sigma_n^4\sum_{j=N-v+1}^{N-1}w_{1,m}^j\sum_{z=j+1}^{N}w_{1,m}^z
\end{aligned}
\tag{59}
$$

[2] L. Xiang, X. Ge, C. -X. Wang, F. Y. Li and F. Reichert, "Energy Efficiency Evaluation of Cellular Networks Based on Spatial Distributions of Traffic Load and Power Consumption," IEEE Transactions on Wireless Communications, vol. 12, no. 3, pp. 961-973, March 2013.

[3] D. Niyato and E. Hossain, "Spectrum trading in cognitive radio networks: A market-equilibrium-based approach," IEEE Wireless Communications, vol. 15, no. 6, pp. 71-80, December 2008.

[4] X. Liu, M. Jia, Z. Na, W. Lu, and F. Li, "Multi-Modal Cooperative Spectrum Sensing Based on Dempster-Shafer Fusion in 5G-Based Cognitive Radio," IEEE Access, vol. 6, pp. 199-208, 2018..

[5] B. Kumar, S. K. Dhurandher, and I. Woungang, "A survey of overlay and underlay paradigms in cognitive radio networks," International Journal of Communication Systems, vol. 31, no. 2, Jan 25 2018, Art. no. e3443.

[6] X. Liu, K. Zheng, K. Chi, and Y. H. Zhu, "Cooperative Spectrum Sensing Optimization in Energy-Harvesting Cognitive Radio Networks," IEEE Transactions on Wireless Communications, vol. 19, no. 11, pp. 7663-7676, 2020.

[7] X. Ge, J. Ye, Y. Yang and Q. Li, "User Mobility Evaluation for 5G Small Cell Networks Based on Individual Mobility Model," IEEE Journal on Selected Areas in Communications, vol. 34, no. 3, pp. 528-541, March 2016.

[8] Y. Zhong, T. Q. S. Quek and X. Ge, "Heterogeneous Cellular Networks With Spatio-Temporal Traffic: Delay Analysis and Scheduling," IEEE Journal on Selected Areas in Communications, vol. 35, no. 6, pp. 1373-1386, June 2017.

[9] I. F. Akyildiz, B. F. Lo, and R. Balakrishnan, "Cooperative spectrum sensing in cognitive radio networks: A survey," Physical Communication, vol. 4, no. 1, pp. 40-62, Mar 2011.

[10] A. S. Rawat, P. Anand, H. Chen, and P. K. Varshney, "Collaborative Spectrum Sensing in the Presence of Byzantine Attacks in Cognitive Radio Networks," IEEE Transactions on Signal Processing, vol. 59, no. 2, pp. 774-786, Feb 2011.

[11] S. Nakamoto, "Bitcoin: A Peer-to-Peer Electronic Cash System," 2009.

[12] M. Belotti, N. Boi, G. Pujolle and S. Secci, "A Vademecum on Blockchain Technologies: When, Which, and How," IEEE Communications Surveys& Tutorials, vol. 21, no. 4, pp. 3796-3838, Fourthquarter 2019.

[13] B. Cao et al., "Performance analysis and comparison of PoW, PoS and DAG based blockchains," Digital Communications and Networks, vol. 6, no. 4, pp. 480-485, Nov 2020.

[14] Popov S, "The tangle, White paper, Online available: https://www.iota.org/research/academic-papers.

[15] Y. Li et al., "Direct Acyclic Graph-Based Ledger for Internet of Things: Performance and Security Analysis," IEEE ACM Transactions on Networking, vol. 28, no. 4, pp. 1643-1656, Aug 2020.

[16] J. M. Lasry and P. L. Lions, "Mean field games," Japanese Journal of Mathematics, vol. 2, no. 1, pp. 229-260, 2007.

[17] M. Huang, P. E. Caines and R. P. Malhame, "Large-Population Cost-Coupled LQG Problems With Nonuniform Agents: Individual-Mass Behavior and Decentralized ε-Nash Equilibria," IEEE Transactions on Automatic Control, vol. 52, no. 9, pp. 1560-1571, Sept. 2007.

[18] M. Huang, R. P. Malhame, P. E. J. C. i. I. Caines, and Systems, "Large population stochastic dynamic games: Closed-loop McKean-Vlasov systems and the Nash certainty equivalence principle," Communications in Information & Systems, vol. 6, no. 3, pp. 221-251, 2006.

[19] P. Semasinghe and E. Hossain, "Downlink Power Control in Self-Organizing Dense Small Cells Underlaying Macrocells: A Mean Field Game," IEEE Transactions on Mobile Computing, vol. 15, no. 2, pp. 350-363, Feb 2016.

[20] S. Samarakoon, M. Bennis, W. Saad, M. Debbah, and M. Latva-Aho, "Ultra Dense Small Cell Networks: Turning Density Into Energy Efficiency," IEEE Journal on Selected Areas in Communications, vol. 34, no. 5, pp. 1267-1280, May 2016.

[21] C. G. Yang, J. D. Li, P. Semasinghe, E. Hossain, S. M. Perlaza, and Z. Han, "Distributed Interference and Energy-Aware Power Control for Ultra-Dense D2D Networks: A Mean Field Game," IEEE Transactions on Wireless Communications, vol. 16, no. 2, pp. 1205-1217, Feb 2017.

[22] R. Sarikhani and F. Keynia, "Cooperative Spectrum Sensing Meets Machine Learning: Deep Reinforcement Learning Approach," IEEE Communications Letters, vol. 24, no. 7, pp. 1459-1462, July 2020.

[23] A. Gao, C. Du, S. X. Ng and W. Liang, "A Cooperative Spectrum Sensing With Multi-Agent Reinforcement Learning Approach in Cognitive Radio Networks," IEEE Communications Letters, vol. 25, no. 8, pp. 2604-2608, Aug. 2021.

[24] Z. Chen, Y. -Q. Xu, H. Wang and D. Guo, "Federated Learning-Based Cooperative Spectrum Sensing in Cognitive Radio," IEEE Communications Letters, vol. 26, no. 2, pp. 330-334, Feb. 2022.

[25] H. Chen, Z. Wang and L. Zhang, "Collaborative spectrum sensing for illegal drone detection: A deep learning-based image classification perspective," China Communications, vol. 17, no. 2, pp. 81-92, Feb. 2020.

[26] P. Cai, Y. Zhang and C. Pan, "Coordination Graph-Based Deep Reinforcement Learning for Cooperative Spectrum Sensing Under Correlated Fading," IEEE Wireless Communications Letters, vol. 9, no. 10, pp. 1778-1781, Oct. 2020.

[27] X. Liu and X. Tan, "Optimization algorithm of periodical cooperative spectrum sensing in cognitive radio," International Journal of Communication Systems, vol. 27, no. 5, pp. 705-720, May 2014.

[28] N. Gupta, S. K. Dhurandher, and A. Sehgal, "A Contract Theory Approach-Based Scheme to Encourage Secondary Users for Cooperative Sensing in Cognitive Radio Networks," IEEE Systems Journal, vol. 14, no. 2, pp. 2400-2410, Jun 2020.

[29] R. Muthukkumar and D. Manimegalai, "Enhanced Cooperative Spectrum Sensing in CRAHNs Using Distributed Dynamic Load-Balanced Clustering Scheme," Wireless Personal Communications, vol. 94, no. 4, pp. 2513-2531, Jun 2017.

[30] B. B. Wang, Y. L. Wu, and K. J. R. Liu, "Game theory for cognitive radio networks: An overview," Computer Networks, vol. 54, no. 14, pp. 2537-2561, Oct 2010.

[31] X. H. Li and Q. Zhu, "Game based incentive mechanism for cooperative spectrum sensing with mobile crowd sensors," Wireless Networks, vol. 25, no. 4, pp. 1855-1866, May 2019.

[32] Z. S. Jiang, W. Yuan, H. Leung, X. G. You, and Q. Zheng, "Coalition Formation and Spectrum Sharing of Cooperative Spectrum Sensing Participants," IEEE Transactions on Cybernetics, vol. 47, no. 5, pp. 1133-1146, May 2017.

[33] W. U. Mondal, A. A. Sardar, N. Biswas, and G. Das, "Nash Bargaining-Based Economic Analysis of Opportunistic Cognitive Cellular Networks," IEEE Transactions on Cognitive Communications and Networking, vol. 6, no. 1, pp. 242-255, Mar 2020.

[34] M. A. A. Careem and A. Dutta, "SenseChain: Blockchain based Reputation System for Distributed Spectrum Enforcement," 2019 IEEE International Symposium on Dynamic Spectrum Access Networks (DySPAN), 2019, pp. 1-10.

[35] T. Huang, X. Li, and X. Ying, "A Blockchain-Based Node Selection Algorithm in Cognitive Wireless Networks," IEEE Access, vol. 8, pp. 207156-207166, 2020.

[36] Y. Pei, S. Hu, F. Zhong, D. Niyato and Y. -C. Liang, "Blockchain-Enabled Dynamic Spectrum Access: Cooperative Spectrum Sensing, Access and Mining," 2019 IEEE Global Communications Conference (GLOBECOM), 2019, pp. 1-6..

[37] S. Nallagonda, A. Chandra, S. D. Roy, S. Kundu, P. Kukolev, and A. Prokes, "Detection performance of cooperative spectrum sensing with hard decision fusion in fading channels," International Journal of Electronics, vol. 103, no. 2, pp. 297-321, Feb 1 2016.
[38] A. A. Olawole, F. Takawira, and O. O. Oyerinde, "Fusion rule and cluster head selection scheme in cooperative spectrum sensing," IET Communications, vol. 13, no. 6, pp. 758-765, Apr 2019.
[39] H. F. Lin, L. Du, and Y. F. Liu, "Soft Decision Cooperative Spectrum Sensing With Entropy Weight Method for Cognitive Radio Sensor Networks," IEEE Access, vol. 8, pp. 109000-109008, 2020.
[40] S. Nallagonda, Y. R. Kumar and P. Shilpa, "Analysis of Hard-Decision and Soft-Data Fusion Schemes for Cooperative Spectrum Sensing in Rayleigh Fading Channel," 2017 IEEE 7th International Advance Computing Conference (IACC), 2017, pp. 220-225.
[41] H. M. Soner, "Controlled Markov processes, viscosity solutions and applications to mathematical finance," Viscosity Solutions and Applications, vol. 1660, I. C. Dolcetta and P. L. Lions, Eds. (Lecture Notes in Mathematics, 1997, pp. 134-185.
[42] S. Bae and H. Kim, "Unlimited cooperative sensing with energy detection for cognitive radio," Journal of Communications and Networks, vol. 16, no. 2, pp. 172-182, 2014.
[43] F. Meriaux, S. Lasaulce, and H. Tembine, "Stochastic Differential Games and Energy-Efficient Power Control," Dynamic Games and Applications, vol. 3, no. 1, pp. 3-23, Mar 2013.
[44] D. Jiang, G. F. Li, Y. Sun, J. Y. Kong, and B. Tao, "Gesture recognition based on skeletonization algorithm and CNN with ASL database," Multimedia Tools and Applications, vol. 78, no. 21, pp. 29953-29970, Nov 2019.
[45] Y. Li et al., "Direct Acyclic Graph-Based Ledger for Internet of Things: Performance and Security Analysis," IEEE/ACM Transactions on Networking, vol. 28, no. 4, pp. 1643-1656, Aug. 2020.
[46] X. Ge, H. Jia, Y. Zhong, Y. Xiao, Y. Li and B. Vucetic, "Energy Efficient Optimization of Wireless-Powered 5G Full Duplex Cellular Networks: A Mean Field Game Approach," IEEE Transactions on Green Communications and Networking, vol. 3, no. 2, pp. 455-467, June 2019.
[47] Y. Liu, S. Qin, Y. Sun, G. Feng, "Resource Consumption for Supporting Federated Learning in Wireless Networks," arXiv preprint arXiv:2204.03850, 2022.

Shuang Zheng received the Masters degree in electronic information and communications from the Huazhong university of science and technology, Wuhan, China, in 2021. Her research interests are Spectrum sharing and blockchain technology.

Yuna Jiang received the B.E. degree in communications engineering from the China University of Mining and Technology, Xuzhou, China, in 2017. She is currently working toward the Ph.D. degree with the School of Electronic Information and Communications, Huazhong University of Science and Technology. Her research interests are blockchain and resource allocation in Internet of Things networks.

Xiaohu Ge (M'09-SM'11) is currently a full Professor with the School of Electronic Information and Communications at Huazhong University of Science and Technology (HUST), China. He is an adjunct professor with the Faculty of Engineering and Information Technology at University of Technology Sydney (UTS), Australia. He received his PhD degree in Communication and Information Engineering from HUST in 2003. He has worked at HUST since Nov. 2005. Prior to that, he worked as a researcher at Ajou University (Korea) and Politecnico Di Torino (Italy) from Jan. 2004 to Oct. 2005. His research interests are in the area of mobile communications, traffic modeling in wireless networks, green communications, and interference modeling in wireless communications. He has published more than 200 papers in refereed journals and conference proceedings and has been granted about 50 patents in China. He received the Best Paper Awards from IEEE Globecom 2010. Dr. Ge services as the China Representative for international federation for information processing (IFIP). He serves as an associate editor for *IEEE Wireless Communications*, *IEEE Transactions on Vehicular Technology* and *IEEE ACCESS*, etc. He served as the general Chair for the 2015 IEEE International Conference on Green Computing and Communications (IEEE GreenCom 2015).

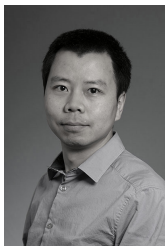

Yong Xiao (S'09-M'13-SM'15) is a professor in the School of Electronic Information and Communications at the Huazhong University of Science and Technology (HUST), Wuhan, China. He is also the associate group leader of the network intelligence group of IMT-2030 (6G promoting group) and the vice director of 5G Verticals Innovation Laboratory at HUST. Before he joins HUST, he was a research assistant professor in the Department of Electrical and Computer Engineering at the University of Arizona where he was also the center manager of the Broadband Wireless Access and Applications Center (BWAC), an NSF Industry/University Cooperative Research Center (I/UCRC) led by the University of Arizona. Prior to that, he worked as a Postdoc Research Fellow at Trinity College Dublin, Massachusetts Institute of Technology, and University of Houston. His research interests include machine learning, game theory, distributed optimization, and their applications in cloud/fog/mobile edge computing, semantic communications, green communication systems, wireless communication networks, and Internet-of-Things (IoT).

Yang Huang received the B.S. and M. S. degrees from Northeastern University, China, in 2011 and 2013, respectively, and the Ph.D. degree from Imperial College London in 2017. He is currently an Associate Professor with College of Electronic and Information Engineering, Nanjing University of Aeronautics and Astronautics, Nanjing, China. His research interests include wireless communications, MIMO systems, convex optimization, machine learning and signal processing for communications. He has served as Technical Program Committee (TPC) members for many International conferences, such as IEEE GLOBECOM, etc.

Yuan Liu (S11-M13-SM18) received the B.S. degree from Hunan University of Science and Technology, Xiangtan, China, in 2006; the M.S. degree from Guangdong University of Technology, Guangzhou, China, in 2009; and the Ph.D. degree from Shanghai Jiao Tong University, China, in 2013, all in electronic engineering. Since 2013, he has been with the School of Electronic and Information Engineering, South China University of Technology, Guangzhou, where he is currently an associate professor. Dr. Liu serves as an editor for the IEEE COMMUNICATIONS LETTERS and the IEEE ACCESS. His research interests include 5G communications and beyond, mobile edge computation offloading, and machine learning in wireless networks.